Modelling of reverse electrodialysis in the presence of multivalent ions

Werges, Yuris I.

Award date:
2022

Modelling of reverse electrodialysis in the presence of multivalent ions

Master thesis

March 2021

Yuris I. Werges

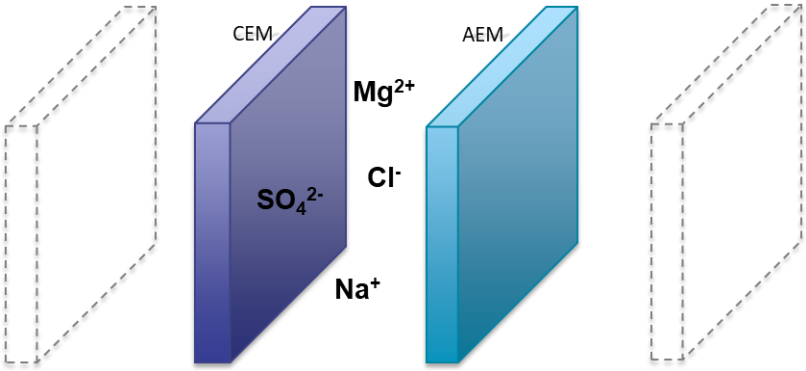

Graduation committee:

prof. dr. ir. K. Nijmeijer

prof dr.ir. Z. Borneman

dr. ir. K. Buist

D. Pintossi

March 2, 2021

TU/E

Abstract

The growing need for sustainable energy to mitigate climate change has increased research efforts for sustainable energy sources. Salinity gradient energy as a clean source of energy can be harvested using reverse electrodialysis (RED). RED faces a major challenge in the prevention of fouling, which is detrimental to the process performance. Multivalent ions are one cause for reduced process performance and modelling their presence can be useful for future RED development and fouling prevention.

A model was developed based on existing literature, to predict RED membrane performance in the presence of multivalent ions. It was based on the Nernst-Planck equation, including Donnan equilibrium. In combination with Vermaas' uphill transport model, the effects of uphill transport, permselectivity loss and increased resistance can all be covered by the model. Permselectivity predictions were made using the model and compared to experimental data. Using only a single fitting parameter, good agreement with experimental results was found.

Contents

Abstract 1
Contents 2
Nomenclature 4
1 Introduction 6
1.1 RED principles 7
1.1.1 Fouling 10
1.2 Multivalent ions 10
1.3 Modelling approaches 11
1.4 Research goal 14
2 Theory 15
2.1 Electroneutrality 15
2.2 Nernst-Planck 15
2.2.1 Diffusion coefficients 16
2.2.2 Convection 16
2.2.3 Electric field 17
2.3 Donnan equilibrium 19
2.3.1 Solving the D-EN equilibrium equation 21
2.3.2 Steric, Electric, Di-Electric model 21
2.4 Nernst equation 22
2.4.1 Permselectivity 23
2.5 Uphill transport 24
3 Model description 25
3.1 Membrane model 25
3.1.1 Governing equations 25
3.1.2 Boundary conditions 27
3.1.3 Diffusion and activity coefficients 28
3.1.4 Discretization 29
3.2 Nernst uphill transport model 29
4 Methods 31
4.1 Solution method 31
4.2 Simulations 32
5 Results and discussion 34

5.1 Uphill transport 34
5.1.1 Nernst equation 34
5.1.2 Membrane model 36
5.1.3 OCV loss through uphill transport 39
5.2 Permselectivity 40
5.2.1 Feedwater composition 40
5.2.2 Charge density 41
5.2.3 Experimental fit 42
5.2.4 Convection 44
6 Conclusion 45
7 Future work 47
8 Acknowledgement 49
9 Bibliography 50
Appendix A. Model flowchart 57
Appendix B: Model comparison for NaCl 58

Nomenclature

List of abbreviations

AEM	Anion exchange membrane	SGE	Salinity gradient energy
CEM	Cation exchange membrane	RED	Reverse electrodialysis
SEDE	Steric, electric, di-electric (model)	NP	Nernst-Planck (flux equation)
D-EN	Donnan-electroneutrality		
OCV	Open circuit voltage		

a_i	Activity of component i [mol/m^3]
c_i	Concentration of component i [mol/m^3]
D_i	Diffusion coefficient component i [m^2/s]
dV	Discrete volume (finite volume method) [m^3]
dA	Side area of discrete volume (finite volume method) [m^2]
d_m	Membrane thickness [m]
dx	Discretization interval [m]
E	Electric field [C/m]
F	Faraday's constant [C/mol]
f_{steric}	Steric Mackie-Meares diffusion factor []
f_{fit}	Fitting diffusion factor
J_i	Flux of component i [mol/m^{2}s]
I	Current density [A/m^2]
k	Donnan partition coefficient [-]
L	Length of the membrane(s) and channel(s) in y direction [m]
m, M	Subscript or superscript referring to membrane phase

n	Number of components in the system [-]
P_w	Water permeance [m^3/m^2.bar.s]
P_H	Hydraulic pressure
q	Elementary charge [C]
R	Universal gas constant [J/mol.K]
s, S	Subscript or superscript referring to solution phase
T	Temperature [K]
V_{th}	Theoretical maximum (Nernst) voltage [V]
v	Velocity [m/s]
x_{up}	Concentration change necessary to reach the equilibrium during uphill transport
X_r	Relative charge density (w.r.t. original value) [-]
X_m/X_M	Fixed membrane charge density [mole/m^3 solution in membrane]
z_i	Valency of component i [-]
α	Apparent permselectivity [-]
ε	Electric permittivity [F/m]
γ_i	Activity coefficient of component i [-]
ϕ_w	Volume fraction of water in membrane [-]
$\Delta\phi_D$	Donnan potential [V]
ρ_q	Charge density [C/m^3]
μ_i	Electrochemical potential of component i [$J.mol^{-1}$]
μ_i^0	Reference electrochemical potential of component i [$J.mol^{-1}$]

1 Introduction

To reduce global warming and climate change, the reduction of greenhouse gas emission is of the highest importance. Renewable, clean energy sources play an essential role herein, as they typically have low or zero net emissions. To meet future climate goals, an energy transition towards to renewable sources and away from fossil fuels is necessary [1].

One of these renewable energy sources that has received a steep increase in interest over the last decades is salinity gradient energy (SGE). It is an emerging technology for harvesting the potential energy of mixing that is present when there is a difference in salinity between two solutions [2]. One solution has a high concentration of salt, while the river water has a low concentration of salt, resulting in a salinity gradient where the water bodies meet. These salinity gradients occur naturally, for example where there is an outflow of fresh river water into the sea, such as is the case in river estuaries. Seawater has a high salt concentration, while the river water has a low salt concentration. The energy of mixing seawater and river water can be harvested through the controlled mixing of the two solutions.

The theoretical global capacity of SGE from estuaries has been estimated numerous times, with initial studies pointing to a total of 1.4 or 2.6 TWh [3]. However, the most recent work by Alvarez-Silva et al. quantified not just the theoretical maximum capacity, but also the practical available capacity. The practical capacity was based on the suitability, sustainability and reliability of the river mouths and came to an annual global capacity of 625 TWh for energy production from river estuaries [3]. This is equivalent to about 2.3% of global electricity production in 2018, which is considerably smaller than the theoretical capacity. Nevertheless, it is a significant amount of sustainable energy that should not be neglected as part of the transition to renewable energy sources. In addition to natural salinity gradients, artificial salinity gradient such as industrial concentrated brines, or even engineered salinity gradients can also be used as an SGE source [4], so the potential for SGE is far from limited. The focus in this current work will be on the SGE from natural resources, specifically the conditions found here in the Netherlands at the Wadden Sea and Lake Ijssel.

There are a variety of techniques for producing energy from salinity gradients. The most promising of these techniques were covered in a recent review by Yip et al [5]. Reverse electrodialysis (RED), pressure-retarded osmosis (PRO) and capacitive mixing showed most potential, but still have challenges to tackle before they can be competitive [5–7]. In the current work, a contribution to the challenge of RED will be made.

The following sections will introduce the principles of RED and the challenges met by the presence of multivalent ions. Modelling approaches and the goal of the current work will be covered afterwards.

1.1 RED principles

In a RED cell, alternating anion exchange membranes (AEMs) a cation exchange membranes (CEMs) are stacked on top of each other. Between the membranes are spacers that create feedwater channels for salt solutions. A high concentration salt solution, seawater, and a low concentration salt solution, river water, flow through these channels and ions transfer from the high concentration seawater (SW) to the low concentration river water (RW) solution, see **Figure 1**. The positive ions pass preferably through the CEM on one side of the channel, while the negative ions pass preferably through the AEM on the other side of the channel.

This ability of AEMs and CEMs to transport one specific type of charge is based on fixed charges, covalently bound inside the membranes. An AEM will be positively charged and will therefore reject positively charged ions (the co-ions) and attract negatively charged ions (the counter-ions). For a CEM the fixed membrane charge is negative and the co-ions and counter-ions are reversed. The effectiveness with which counterions are transported through the membrane while co-ions are excluded and is referred to as the permselectivity, which is an important parameter for identifying membrane performance.

This electrostatic effect of co-ion exclusion was first described and published by Donnan in 1924 and is now referred to as Donnan exclusion [11]. The result of Donnan exclusion is that an electrical potential develops across the membranes, which is required for electrical power production. The second requirement, a current, is met because positive ions move in one direction and negative ions in the other. Hence, a net movement of charge (ion current) develops in one direction. This ion current is converted at the electrodes into an electric current by redox reactions, which can be used for power applications, see **Figure 1**.

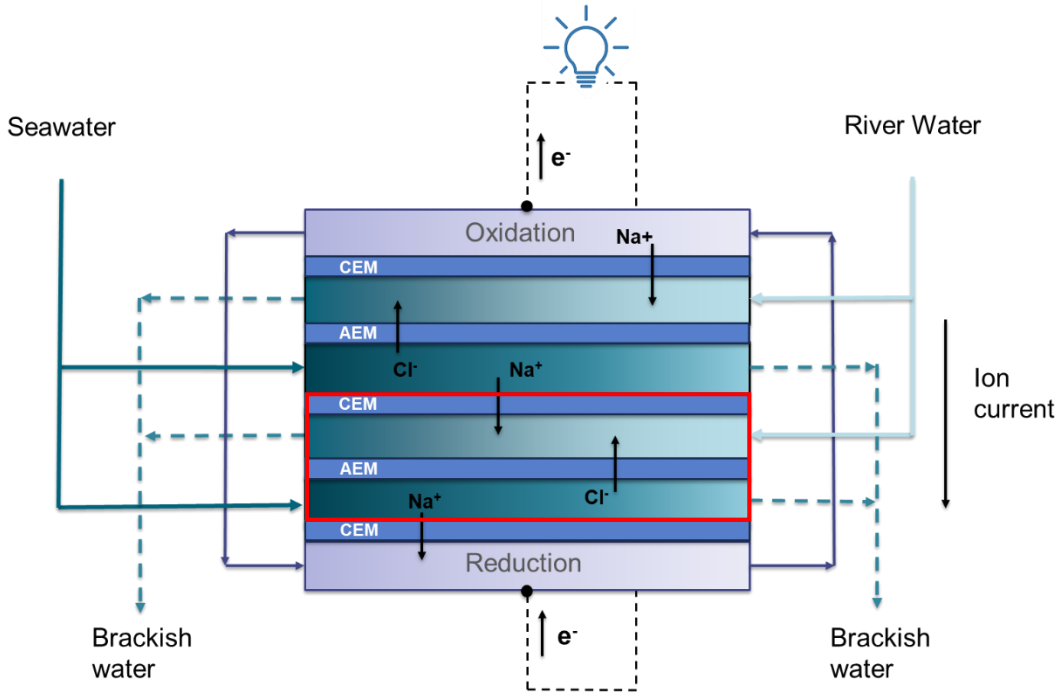

Figure 1. Schematic of the working principle of an RED stack. The red-outlined section is the unit cell which can be repeated to increase the overall voltage of the stack. It consists of a seawater channel, river water channel and a CEM and AEM. At one side, an extra membrane is placed to separate the electrode electrolyte solution from the feedwaters.

The feedwaters can be pumped through the channels in different directions. The flow configuration is called co-flow when both flow the same direction, counter-flow when they flow in opposite directions and cross-flow when they flow perpendicular to each other, see **Figure 2**. The flow configuration affects the energy efficiency of the system because it influences the average salinity gradient that is present in the cells. Specifically, counter-flow has the highest efficiency across the entire channel. Because the outflows are on opposite sides of the channels, even when outflow concentrations are the same, a salinity gradient across the membranes persists along the entire channel. In co-flow

configuration the electromotive force is initially larger, but the salinity difference across the membranes will decrease faster and it will reach zero when outflow concentrations are the same. This results in a larger amount of unused energy and thus lower efficiency [12]. This principle is similar to the well-known case for heat exchangers, where a counterflow heat exchanger will (usually) have the best performance because it has the largest average temperature difference between the two heat-exchanging phases and being able to extract more heat. Cross-flow is a mix of the two therefore having energy efficiencies slightly lower than that of counter-flow but higher than co-flow [12].

Besides the flow mode, the power output depends on many other parameters such as the membrane properties, feedwater composition and general process parameters like flow rate, temperature etc. The voltage between the electrodes also influences performance and it was shown very recently by Simoes et al. that segmentation of the electrodes can improve power density by almost 40% [12,13]. Optimization of the voltages over a segmented electrode can provide significant improvement of both power density and energy efficiency, related to the capital and operational costs, respectively [13].

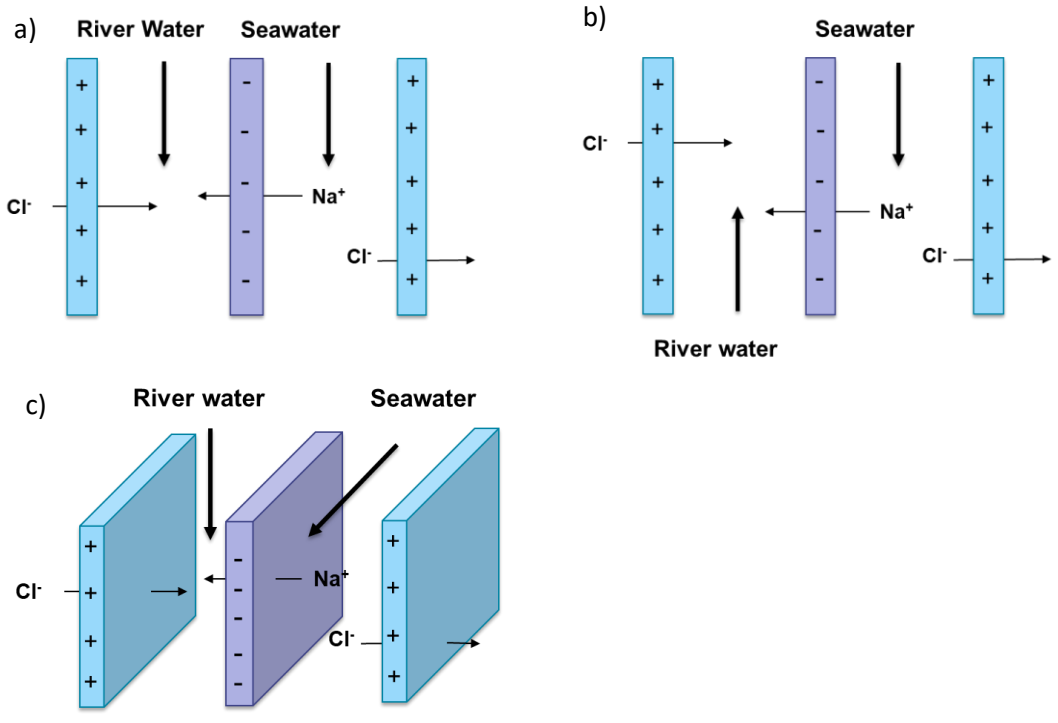

Figure 2. Flow configurations in RED. a) co-flow, b) counter-flow, c) cross-flow.

1.1.1 Fouling

When dealing with natural feedwaters, as is often the case for RED, the power output can be significantly lower than when dealing with artificial solutions. Natural waters contain organic particles, clay particles, micro-organisms and multivalent ions [14]. All of these can negatively influence the performance of RED, which is called fouling. Fouling can be, for example, clogging of the channels, scaling of the membrane or other negative interactions with the membrane. The reduction of fouling is a major challenge to improve the real-world performance of RED.

1.2 Multivalent ions

Fouling also originates from the presence of multivalent ions. They pose a significant challenge as they negatively influence the membrane in three ways:

- increased membrane resistance
- loss of permselectivity
- loss of potential through uphill transport.

Most of these performance losses are observed instantly, but there can also be long-term detrimental effects to the membranes, as shown by Pintossi et al.[14].

An immediate increase in membrane resistance is observed when multivalent ions are added to RED solutions because generally, there is a higher resistance to transport of multivalent ions than there is to monovalent ions. The reason for this higher resistance is that multivalent ions have a larger hydrated radii and a smaller free energy of hydration (they form stronger hydrogen bonds with the water molecules surrounding them) [14,15]. This hinders transport through the membrane.

Furthermore, the presence of multivalent ions will instantly result in a loss of permselectivity because Donnan exclusion is less effective when multivalent ions are present [16]. It is also possible for multivalent ions to bond to a single fixed charge, reversing it and reducing the ion exchange capacity and permselectivity of the membrane [14].

Lastly, uphill transport is also a direct effect of multivalent ions. Multivalent ions can travel through the membrane against their external concentration gradient, from a solution with a low concentration

to a higher concentration solution. In exchange, monovalent ions are moved from the high concentration to the low concentration, which results in no net current from one compartment to the other. This is referred to as the uphill transport of multivalent ions. In theory, uphill transport is also possible for monovalent ions, but this is not the case for natural salinity gradients. Uphill transport of multivalent ions leads to a reduced potential gradient between the two compartments and a significant loss of power output [14,16–18].

Long term losses originate from the stronger ionic interactions multivalent ions have with the fixed charges inside the membrane. Multivalent ions can become 'trapped' in the membrane, binding to multiple fixed charges in the membrane and neutralizing them. This is referred to as 'poisoning' of the membrane. It increases membrane resistance over time, because of the reduced free volume available for transport and a reduced ion charge density. This lower charge density in the membrane also lowers the permselectivity.

The increased membrane resistance and loss of permselectivity may be understood more intuitively than the phenomenon of uphill transport; ions moving against an external concentration gradient seems in conflict with Fick's law of diffusion. Hence, it will be discussed it in more detail in theory section 2.5.

1.3 Modelling approaches

So far, a variety of different modelling approaches has been used to model the transport mechanisms present in RED. Most of these are based on the (extended) Nernst-Planck (NP) equation coupled with either the Donnan equilibrium [16,19], the steric electric di-electric (SEDE) model [20] or the Poisson equation [21]. Other work is based on irreversible thermodynamics [22], Maxwell-Stefan diffusion or semi-empirical models using overall membrane properties [13,23–25].

The most inclusive of the modelling frameworks are the irreversible thermodynamics and Maxwell-Stefan approaches, but they have the drawback that they require a lot of parameters that can be difficult to acquire experimentally. While the Nernst-Planck approach cannot fully fill the role of an all-inclusive theoretic basis for ionic transport [22], it is nevertheless a more fundamental approach

than the semi-empirical models. When combined with the Einstein(-Smoluchowsky) relation it requires only a few membrane properties and one diffusion coefficient per ion, per phase (solution, membrane), making it more accessible than more fundamental approaches [26]. The focus for the current will be on the theoretical framework for dealing with multivalent ions and their effect on (simulated) membrane performance, so the more accessible approach of the NP equation will be used. In most published models, electroneutrality is assumed, with the exception being when the Poisson equation is used for solving the electric field and the membrane-solution interface [21,27]. However, electroneutrality in combination with the Donnan equilibrium to account for the local potential jump that occurs at the membrane interface is the most common approach [16,26,28–30].

Tedesco et al. published three works on Nernst-Planck theory for reverse electrodialysis [28,31,32]. They showed the effect of transport of co-ions, water (osmotic) and optimal membrane thickness, but considered a monovalent-ion system only. While the work by Tedesco can be considered a benchmark for NP based RED modelling, it did not consider the effect of more realistic feedwaters including multivalent ions.

In fact, there is little modelling work to be found on RED with multi-ionic, multivalent systems. Gi Hong et al. investigated the effect of multivalent ions in a semi-empirical model, but this approach does not offer a theoretical framework for observed permselectivity decrease or uphill transport in the presence of multivalent ions [14,17]. Recently, Moya described uphill transport in a CEM using a Donnan-Nernst-Planck based approach which had a much better theoretical basis [16].

The model developed by Moya showed promising behavior. It was able to predict uphill transport and provide possible process improvements based on the models results. However, the predictions of Moya's work were purely theoretical and it included assumptions for the membrane properties and diffusion coefficients in the membrane. The assumptions were reasonable, based on experimentally observed relations for the diffusion coefficients, but they were not validated as such.

Furthermore, the work of Moya showed no predictions for the permselectivity of the simulated membrane in the presence of multivalent ions and it omitted the study of divalent anions and AEMs.

Rijnaarts et al. showed that fouling due to multivalent ions has the most effect on the CEMs, but Pintossi et al. highlighted the fact that also AEMs are significantly influenced by the presence of multivalent ions [14,17]. Hence, the theoretical study of AEMs is also deemed relevant and may be a step forward to developing a more complete RED process performance model. To the best of our knowledge, no Nernst-Planck based model has been published investigating AEMs or a full RED system with both membranes in presence of multivalent ions.

The simulation of multi-ionic systems is however not limited to RED. Moshtarikhah et al. covered a NP based simulation of a Nafion membrane for NF applications [33], and in the field of electrodialysis, multicomponent mixtures are more commonly found in recent publications [29,34]. These last two works by Yip et al. [29] and Honarparvar and Reible [34] show great similarity to the Donnan-Nernst-Planck approach adopted by Moya [16].

Another interesting study that is useful the field of RED, is that of Kingsbury and Coronell [30]. They modelled the concentration dependence of the permselectivity of ion exchange membranes using the Donnan-Nernst-Planck approach. Their model was validated and showed great promise predicting the experimental permselectivity data of a variety of membranes. While not exclusively aimed at RED, the permselectivity is a very important parameter for determining the performance in RED. Unfortunately, Kingsbury and Coronell only covered the dependence of permselectivity on NaCl solutions, omitting the study of multivalent ions.

In conclusion: Moya showed the capability of the Donnan-Nernst-Planck approach to include the effects of multivalent ions, but lacked experimental validation in the form of, for example, apparent permselectivity measurements [16]. Kingsbury and Coronell, using a similar modelling strategy, showed the validity of the same approach in predicting permselectivity, but omitted the study of multivalent ions [30]. In the current work, an attempt will be made to cover gaps between these two studies in a RED context.

1.4 Research goal

The goal of this research is to model the permselectivity of RED membranes in the presence of multivalent ions, while accounting for uphill transport. Providing insight in the way the Donnan-Nernst-Planck based approach accounts for the experimentally observed effect of multivalent ions. The ultimate aim of the model will be, like any model, to aid the future development and optimization of RED.

2 Theory

2.1 Electroneutrality

The water compartments and membranes in RED adhere to the electroneutrality (EN) constraint. EN is an accurate approximation for the entire system, except for the nanoscale region at the interface between membrane and solution [28]. This phenomenon will be covered in section 2.3. First, the condition of electroneutrality is introduced:

$$\begin{aligned} \sum_{1}^{n} z_i c_i^S &= 0 \qquad \text{(solution)} \\ \sum_{1}^{n} z_i c_i^M + X_m &= 0 \qquad \text{(membrane phase)} \end{aligned} \tag{1}$$

Where the membrane fixed charge density X_m [mol eq.m^{-3}] is 0 in the water compartments, $X_m > 0$ for AEMs and $X_m < 0$ for CEMs. It is important to note here that the definition of the charge density is used per unit volume of absorbed water in the membrane and not per total membrane volume, the same goes for the concentration of ions inside the membrane phase.

2.2 Nernst-Planck

In the electrochemical modelling of RED and ED, the extended Nernst-Planck equation is most used for the description of the different transport mechanisms: diffusion, convection and migration. It has the advantage that it doesn't require a large number of transport coefficients and membrane data, which have to be measured independently [19,35,36].

In this work the extended Nernst-Planck equation was used to model the transport of ions through a RED membrane. It consists of a diffusion, migration, and convection term. When convection is neglected, the regular Nernst-Planck equation remains.

$$J_i = \overbrace{v\, c_i}^{\text{convection}} - \overbrace{D_i \nabla \cdot c_i}^{\text{diffusion}} \overbrace{- D_i \left(-\frac{F}{RT} z_i c_i E \right)}^{\text{migration}} \tag{2}$$

With v the fluid velocity [m.s^{-1}], c_i the concentration of species i [mol.m-^{3}], D_i the diffusion coefficient for species i [m^2.s^{-1}], F Faraday's constant [C.mol^{-1}], R the universal gas constant [J.mol^{-1} K^{-1}], T the temperature [K], z_i the valence if ion i [-] and E the electric field [C.m^{-1}].

2.2.1 Diffusion coefficients

Diffusion coefficients of ions inside the membrane can be difficult to measure, but they can be approximated from solution diffusion coefficients using the model proposed by Mackie and Meares [30,37,38]. Mackie and Meares assumed that the diffusion coefficient of any ion in the water inside a membrane is the same as in a solution, but that the ion travels a more tortuous pathway, lowering the effective diffusion speed. They related the effective diffusion to the water volume fraction inside the membrane. Introducing the steric coefficient for diffusion through the membrane:

$$f_{steric} = \frac{D^M}{D^S} \tag{3}$$

$$f_{steric} = \left(\frac{\phi_w}{2 - \phi_w} \right)^2 \tag{4}$$

With ϕ_w the volume fraction of water inside the membrane [-], which can be determined experimentally.

2.2.2 Convection

The convective term in the Nernst-Planck equation describes the transport of ions due to the movement of their solvent, water. Ions are moved along within the solvent and although the water permeability may be limited, it cannot always be neglected. The velocity with which water permeates the membrane can be described by the equation suggested by Kingsbury et al. [30]:

$$v = -P_w d_m (\nabla P_T + X_m F\, E) \tag{5}$$

Where P_w is the water permeance of the membrane [$m^3.m^{-2}s^{-1}.bar^{-1}$], d_m the thickness of the membrane [m], P_T the total pressure inside the membrane [bar], X_m the fixed charge density inside the membrane [mol eq.m^{-3}], E the electric field [C.m^{-1}] and F Faraday's constant [C.mol^{-1}].

The total pressure difference over the membrane, as argued by Biesheuvel [39], is given by :

$$\nabla P_T = \nabla P_H - \nabla \pi \tag{6}$$

Where P_H is the hydraulic pressure gradient [bar.m^{-1}], assumed to be zero, and $\nabla\pi$ is the osmotic pressure gradient [bar.m^{-1}].

$$\nabla \pi = \frac{(\pi_{d_m} - \pi_0)}{d_m} \tag{7}$$

Where d_m [m] is the membrane thickness, π_{d_m} is the osmotic pressure at the RW side and π_0 the osmotic pressure at the SW side [bar].

This equation for the fluid velocity was based on the work of Biesheuvel [39] and Yaroshchuk [40], which deal with the flow of electrolyte solutions in porous media. It neglects solvation and gravity effects [39], but includes two important driving forces: the pressure and the electric field [30]. The influence of the electric field on an uncharged fluid might be intuitively unclear, but can be explained. The reasoning is that the local fluid elements inside the membrane are not electroneutral, because there is an excess of counter-ions compensating for the fixed charges in the membrane. In fact, the total charge inside the solution is equally large but opposite to that of the effective fixed charge density inside the membrane, to satisfy the electroneutrality condition inside the membrane. The electric field thus exerts an electrostatic body-force on the locally charged fluid elements [30,39].

2.2.3 Electric field

The inclusion of the electric field has seen multiple approaches. One approach uses the Poisson equation for the electrical potential:

$$-\varepsilon \nabla^2 \phi = \rho_q = F \sum_n z_i c_i \tag{8}$$

With ε the electrical permittivity [C.V^{-1}], ϕ the potential [V] and ρ_q the charge density [C.m^{-3}].

Manzanares et al. [21] used the Poisson equation for modelling the electric double layer at the solution-membrane interface. While their work provides interesting results, it has some technical difficulties and a debatable grid size of less than 1Å, which is smaller than the size of the present ions. To investigate the usability of the Poisson equation, this approach was first pursued in a 1D model with a single membrane between two water compartments. Unfortunately, due to the high value of Faraday's coefficient, even small deviations from electroneutrality (as present in the EDL) caused instabilities in the solution method. These instability issues could be potentially be resolved by applying more rigorous solution methods or numerical techniques to reduce the initial effect of the electric field, but another, simpler and more stable approach was found. Hence, the Poisson approach was rested.

Instead of using the Poisson equation for the electric field, one can also use the current density in the system as a starting point. Previous works have widely adopted this approach [16,29,30,33,34]:

$$I = F \sum_n z_i J_i \tag{9}$$

With I the current density in [A.m^{-2}], F Faraday's constant [C.m^{-1}], z_i the valence of ion i [-] and J_i the flux of ion i [mol.m^{-2}.s^{-1}].

Combining equation (2) with equation (9) and equation (5), the following equation for the electric field can be derived:

$$E = \frac{\frac{I}{F} + \sum_n z_i D_i \nabla c_i - \sum_n z_i c_i P_w d_m \nabla \pi}{\sum_n z_i^2 D_i c_i \frac{F}{RT} + X_m F \cdot P_w d_m} \tag{10}$$

The boundary condition for this electric field is the desired current density I [A.m-^{2}] perpendicular to the membrane, at which the system operates. To obtain the potential profile, one can integrate the electric field:

$$\phi(x) = \int_0^x -E \cdot dx \tag{11}$$

Though this approach is easier and more stable than the Poisson approach, it lacks the inherent ability to show the interfacial behavior that is present at the membrane interface, namely a potential and concentration jump. These jumps can be included through the Donnan equilibrium [26,28,36].

2.3 Donnan equilibrium

The fixed charges of the membrane at the membrane-solution interface create an electric field into the solution and attract counterions through Coulombic interactions. The opposite happens for co-ions, the so-called Donnan exclusion [41]. The result is that an electric double layer (EDL) forms and across this EDL a potential jump occurs, referred to as the Donnan potential.

The Donnan potential can be derived from the Donnan equilibrium assumption for the electrochemical potential on the two sides of the solution-membrane interface [26].

$$\mu_i = \mu_i^0 + RT\ln(a_i) + z_i F\phi \tag{12}$$

Where μ_i is the electrochemical potential of ion i [J.mol^{-1}], μ_i^0 the reference chemical potential [J.mol^{-1}] R the universal gas constant [J.mol^{-1}.K^{-1}], T the temperature [K], a_i the activity of species i in the respective phase [mol.m^{-3}], z_i the valence of i [-], F Faraday's constant [C.mol^{-1}] and ϕ the electrical potential [V].

The first step of derivation is the assumption of local equilibrium. The electrochemical potential in the membrane (M) and inside the solution (S) are equal:

$$\begin{gathered}\mu^S = \mu^M \\ \mu_i^0 + RT\ln\left(a_i^S\right) + z_i F\phi^S = \mu_i^0 + RT\ln\left(a_i^M\right) + z_i F\phi^M\end{gathered} \tag{13}$$

Which can be rewritten as

$$\frac{a_i^S}{a_i^M} = \exp\left(z_i \frac{F}{RT}\left(\phi^M - \phi^S\right)\right) \tag{14}$$

$$\frac{a_i^M}{a_i^S} = \exp\left(-z_i \frac{F}{RT}\Delta\phi_D\right) = k^{z_i} \tag{15}$$

With k the Donnan partition coefficient [-] and $\Delta\phi_D$ the Donnan potential across the membrane-solution interface [V]. Rewriting this, and writing the activity as the product of the activity coefficient and the concentration, gives:

$$\Delta\phi = -\frac{RT}{z_i F} \cdot \ln\left(\frac{\gamma_i^M c_i^M}{\gamma_i^S c_i^S}\right) = -\frac{RT}{F}\ln(k) \tag{16}$$

Where γ_i is the activity coefficient of ion i [-] and c_i the concentration [mol.m^{-3}].

From this equation, the concentration of ion i inside the membrane can be written as:

$$c_i^M = \frac{\gamma_i^S}{\gamma_i^M} c_i^S \cdot k^{z_i} \tag{17}$$

Equation (17) can be used to find the value of the Donnan potential, by combining it with the electroneutrality condition inside the membrane, equation (1):

$$\sum_n z_i \frac{\gamma_i^S}{\gamma_i^M} c_i^S k^{z_i} + X_m = 0 \tag{18}$$

This equation will be referred to as the Donnan-electroneutrality (D-EN) equation.

For a system containing one positive and one negative divalent ion, one positive and one negative monovalent ion, the D-EN equation is written in full as:

$$2\frac{\gamma_{2+}^S}{\gamma_{2+}^M} c_{2+}^S \cdot k^2 + \frac{\gamma_+^S}{\gamma_+^M} c_+^S \cdot k + (-)\frac{\gamma_-^S}{\gamma_-^M} c_-^S \cdot k^{-1} + (-2)\frac{\gamma_{2-}^S}{\gamma_{2-}^M} c_{2-}^S \cdot k^{-2} + X = 0 \tag{19}$$

Where the ions are indicated by their valency ($+$, $-$, …).

This electroneutrality equation with Donnan partition coefficients can be written as a quartic polynomial in the form:

$$ax^4 + bx^3 + cx^2 + dx + e = 0 \tag{20}$$

Where x stands for the Donnan partition coefficient (k), which we can solve for and substitute into equation (16) to find the Donnan potential and calculate the solution composition in the membrane. This method for calculating the membrane composition as a function of the solution composition, activity coefficients and membrane charge density, will be referred to as the Donnan-electroneutrality (D-EN) method, with equation (18) being the general D-EN equilibrium equation.

2.3.1 Solving the D-EN equilibrium equation

The solution to the D-EN equilibrium of a multi-ionic mixture becomes more complex with increasing valency and number of ions and when non-unity activity coefficients are considered. The simplest solution is that of an ideal monovalent mixture, because then D-EN equation (18 is only quadratic:

$$k \cdot c_+ - \frac{c_-}{k} + X = 0 \tag{21}$$

$$k^2 \cdot c_+ + X \cdot k - c_- = 0 \tag{22}$$

$$k = \frac{-X + \sqrt{X^2 + 4 \cdot c_+ c_-}}{2c_+} \tag{23}$$

Where c_+ and c_- are the concentrations [mol.m^{-3}] of positive and negative monovalent ions, respectively, and X is again the fixed charge density in the membrane [mol eq.m^{-3}].

In a mixture of multiple ions with higher valences, the results are higher order equations. In this work, the quartic equation, equation (19), is solved analytically. Higher valences will result in higher order equations which have to be solved numerically. When a non-unity membrane activity coefficient as function of the membrane concentration is considered, the equation may also have to be solved numerically, but in this work that is not the case.

A quartic and cubic solver algorithm based on the solutions of Ferrari and Cardano is used to compute the analytical solutions. It is taken into consideration that a quartic equation will have up to 4 unique solutions, so a choice is made for finding the right solution to the Donnan partition coefficient (k). The only solutions that are allowed, are solutions larger than 0, because negative or imaginary concentration ratios do not exist. Depending on the nature of the membrane the solution to equation (19) will be larger or smaller than one. For CEMs, $k > 1$, because the concentration of counter-ions in the membrane scales linearly with the partition coefficient. For AEMs $k < 1$, because the counter-ion membrane concentration scales inversely with k.

2.3.2 Steric, Electric, Di-Electric model

Besides an electric (Donnan potential) contribution, the Donnan equilibrium relation can also include steric and di-electric effects, to represent the interfacial equilibrium more accurately. Steric effects

can be included in the form of a steric exclusion coefficient, while dielectric effects are established in the form of image forces that arise because of the dielectric difference between the membrane and the solution. This approach has been applied in nanofiltration modelling and could be considered for RED as well [26,41,42]. Equation (15) then takes the following form:

$$\frac{a_i^M}{a_i^S} = \phi_i \exp\left(-z_i \frac{F}{RT} \Delta\phi_D - \Delta W'_{i,im}\right) = k^{z_i} \tag{24}$$

Or, written using activity coefficients:

$$\frac{c_i^M \gamma_i^M}{c_i^S \gamma_i^S} = \phi_i \exp\left(-z_i \frac{F}{RT} \Delta\phi_D - \Delta W'_{i,im}\right) = k^{z_i} \tag{25}$$

Where γ_i is the activity coefficient for either membrane (M) or solution phase (S), Φ_i is the steric exclusion coefficient, z_i, F, R and T have their usual meaning, $\Delta\phi_D$, is the Donnan potential and $\Delta W'_{i,im}$ are the image forces.

The SEDE model requires knowledge of the size of the 'pores' of the membrane for the steric part and knowledge of the dielectric constant of the membrane and solution for the image forces. The dielectric constant is unfortunately ill defined in the nanoscale region where separation happens and depends among other things on the ionic composition of the solution in and outside of the membrane [43,44]. Furthermore, the true nature of the separation mechanism and especially the contribution of dielectric exclusion is still contested, as mentioned by Mohammad et al. [45].

Because the necessary data was unknown and the applicability of the SEDE model is uncertain, the SEDE model was not adopted in the current work. It is still highlighted because it does have the capacity to improve the predictive capabilities of the Donnan model, especially when for example a selective membrane based on steric exclusion is considered [26].

2.4 Nernst equation

To approximate the voltage over an RED membrane at zero current conditions, the open circuit voltage (OCV) of the membrane, can be described using the Nernst equation [18]:

$$V_{OCV} = \alpha \frac{RT}{z_i \cdot F} \ln\left(\frac{a_{sea,i}}{a_{river,i}}\right) = \alpha \frac{RT}{z_i \cdot F} \ln\left(\frac{\gamma_{sea,i} c_{sea,i}}{\gamma_{river,i} c_{sea,i}}\right) \quad (26)$$

Where α is the apparent permselectivity [-], which is higher for a higher fixed charge density in the membrane [46], z_i is the valence of species i [-], a_i is the activity of species i [mol.m^{-3}] in either river or seawater and R, T and F have their usual meaning.

The Nernst equation has been used in previous work for modelling the performance of RED, but it is limited as it doesn't include the effect of the interfacial partitioning of ions or detailed transport mechanisms [13,23,24].

2.4.1 Permselectivity

The 'true' permselectivity of a membrane is based on the measurement of transport numbers from co-ions and counter-ions and is defined as [36]:

$$\alpha_{true} = \frac{t_{cou}^{M} - t_{cou}^{S}}{t_{co}^{S}} \quad (27)$$

Where t_{co} and t_{cou} are the transport numbers [-] of co-ions and counterions in either the solution (S) or membrane (M) phase, given by

$$t_i = \frac{z_i J_i}{\sum z_i J_i} \quad (28)$$

With z_i the valency [-] and J_i the flux [mol.m^{-2}s^{-1}] of component i.

The problem with the true permselectivity is that it is time-consuming to measure experimentally and it is affected by concentration polarization at the membrane interface [36].

A faster method for determining the permselectivity of the membrane, is using the apparent permselectivity. The apparent permselectivity is obtained by measuring the potential gradient over a membrane under static conditions. It can be described by equation (29) [36]:

$$\alpha \cong \frac{V}{V_{th}} \quad (29)$$

Where V is the experimentally measured, potential difference across the membrane [V] and V_{th} is the theoretical Nernst voltage [V].

The apparent permselectivity is also a measure of the effectiveness with which the membrane transports counterions and rejects co-ions. If co-ions are also transported through the membrane, the membrane potential will be lower, which is measured by the apparent permselectivity. Because the apparent permselectivity is much easier to determine and relates directly to the OCV, an important performance parameter, it is widely used to describe membrane performance in combination with the Nernst equation.

Note that in this work, permselectivity and apparent permselectivity are used interchangeably. Except when specifically stated, the 'true' permselectivity is not considered.

2.5 Uphill transport

Uphill transport of multivalent ions against their concentration gradient creates a significant loss of power production in RED. In natural salinity gradients, multivalent ions are present [46] so quantifying and minimizing the loss through uphill transport is important to RED development in natural conditions. Uphill transport has been investigated experimentally and theoretically [14,16–19,47], with different explanations for its occurrence.

Vermaas et al. explain uphill transport by modelling the Nernst equation potential of mono- and divalent ions as two DC generators in parallel. Uphill transport occurs when the electromotive force of the monovalent ions is larger than that of the multivalent ones. The higher voltage generator charges the lower one, until their voltages match. The overall electromotive force is lower, resulting in a loss of power [18].

The explanation using the Donnan equilibrium is different as it depends on the membrane properties. The size of this jump is larger for multivalent ions as they are more strongly attracted by the fixed membrane charges which leads to a (relatively) higher concentration of multivalent ions in the membrane, especially on the river water side. The result of this phenomenon can be that the internal concentration gradient of the membrane is opposite to the external gradient, and therefore the occurrence of uphill transport of multivalent ions.

3 Model description

3.1 Membrane model

The transport of ions through RED membranes was modelled using a one-dimensional model based on the extended Nernst-Planck flux equation. The focus of this model was identifying the occurrence of uphill transport and predicting permselectivity losses due to the presence of multivalent ions. Therefore, the modelling covers the membrane and interfacial phenomena while omitting the feedwater channels and stack-level transport phenomena. The membrane is assumed as a homogeneous membrane phase. The model is one-dimensional and for the water compartments only the interfacial concentration in the solution is considered, modelling the water compartments as ideally mixed with uniform concentrations. **Figure 3** depicts the definition of the model geometry, with an example of a concentration profile inside the membrane. The compositions of the solutions in contact with the membrane are used as inputs to the model.

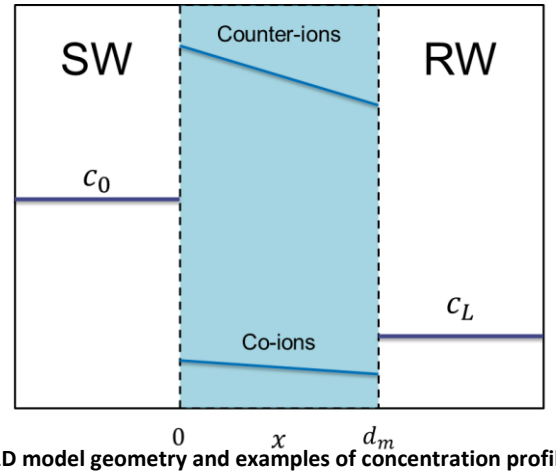

Figure 3. 1D model geometry and examples of concentration profiles

3.1.1 Governing equations

The governing equations are applied through the finite volume method, where the membrane is divided into grid cells of a certain finite volume. For each of these volume elements the mass balance for all ions i is given by:

$$dV\frac{\partial c_i}{\partial t} + dA\left(J_{i,in} - J_{i,out}\right) = 0 \tag{30}$$

Where c_i is the local concentration of component i , $J_{i,in}$ its flux entering the volume [mol.m^{-2}.s^{-1}] and $J_{i,out}$ its flux exiting the volume [mol.m^{-2}.s^{-1}], see **Figure 4**. dV [m^3] and dA [m^2] are the volume and side-area of the finite volume, respectively.

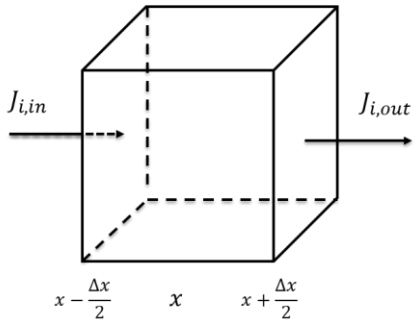

Figure 4. Schematic representation of finite volume method.

In the cases discussed in this work, the model is one-dimensional and operated at steady state, reducing the mass balance to:

$$J_{i,in} - J_{i,out} = 0 \tag{31}$$

3.1.1.1 Ion flux

The flux J_i of component i is given by the extended Nernst-Planck equation, see equation (2):

$$J_i = -D_i\left(\nabla \cdot c_i - \frac{F}{RT} z_i c_i\, E\right) + v\, c_i$$

The electric field is described by equation (10):

$$E = \frac{\frac{I}{F} + \sum_n z_i D_i \nabla c_i - \sum_n z_i c_i P_w \Delta\pi}{\sum_n z_i^2 D_i c_i \frac{F}{RT} + X_m F \cdot P_w d_m}$$

Where the osmotic pressure difference [bar] is given by equation (32)

$$\Delta\pi = \left(\pi_{d_m} - \pi_0\right) \tag{32}$$

And the osmotic pressure (in bar) is approximated by the Van ‘t Hoff equation:

$$\pi = \frac{\sum c_i RT}{10^5} \tag{33}$$

3.1.2 Boundary conditions

For the boundary conditions of the model, constant Dirichlet-type boundary conditions were used for the feedwater concentrations. The concentrations inside the feedwaters is set at a constant value and does not change in time or over the course of model iterations. The reference value of the potential can be chosen, but it is set to 0 on the feedwater-membrane interface that ensures a positive membrane potential output. The current for all performed simulations is set to 0, to simulate OCV conditions.

For all components i:

$$x = 0 \qquad c_i = c_{i,0} \tag{34}$$

$$x = d_m \qquad c_i = c_{i,d_m} \tag{35}$$

Potential

$$x = 0 \qquad \phi = 0 \tag{36}$$

Current

$$I = \sum_{i}^{n} z_i J_i = 0 \tag{37}$$

The electroneutrality condition was also imposed as a constraint on the model. There are several ways of including electroneutrality in an electrochemical model [48], of which the most straightforward one was used. In a system with n ionic species, the concentration of the nth component is determined by the following equation:

$$c_n = -z_n \left(\sum_{1}^{n-1} z_i c_i + X_m \right) \tag{38}$$

The concentrations for the $(n-1)$ other components are determined using the NP equation, by solving their mass balances. It was found that it was generally best for modelling results and convergence that the concentration of the co-ion was used to satisfy the electroneutrality condition.

For the membrane-solution interfacial boundaries, the concentrations at the interface are governed by the electroneutrality condition, equation (1), and the Donnan equilibrium, equation (16), the D-EN method:

$$\sum_{1}^{n} z_i c_i + X_m = 0$$

$$\Delta\phi_D = -\frac{RT}{z_i F} \cdot \ln\left(\frac{\gamma_i^M c_i^M}{\gamma_i^S c_i^S}\right)$$

3.1.3 Diffusion and activity coefficients

The membrane diffusion coefficients were approximated by applying the Mackie and Meares' model [30,38] to the diffusion coefficients in solution given by Table 1. See also equation (4) for the Mackie and Meares model. In addition to the steric factor from the Mackie and Meares model, an additional fit factor is sometimes included to fit the model to experimental data, see equation (39):

$$D_m = f_{fit} f_{steric} D_s \tag{39}$$

Where $D_m$is the membrane diffusion coefficient (specific for each ion) [$m^2.s^{-1}$], f_{fit} the fit factor [-], f_{steric} the steric Mackie and Meares factor [-] and D_s the solution diffusion coefficient [$m^2.s^{-1}$].

Table 1. Ionic diffusion coefficients in solution.

Ion species	$\boldsymbol{Na^+}$	$\boldsymbol{Cl^-}$	$\boldsymbol{SO_4^{2-}}$
Diffusion coefficient solution (m^2/s)	$1.334\ 10^{-9}$	$2.032\ 10^{-9}$	$0.706\ 10^{-9}$

The activity coefficients in the solution were estimated using the three-characteristic-parameter correlation (TCPC) model of Ge et al. The model combines short-range solvation effects with Pitzer long-range interaction and provides the average activity coefficient of a salt [49]. Although data for salt mixtures were not available for this model, it is used as an estimation of the ion activity coefficient. A predictive model for the activity coefficients of arbitrary electrolyte solutions was considered [50], but was refrained from because it added significant, possibly unnecessary, complexity to the model.

For the same reason, the activity coefficient inside the membrane was taken as unity., although there are some works by Kamcev et al. illustrating the use of Mannings counterion condensation theory [37,51,52].

The total potential over the membrane was calculated by integrating the electric field, equation (11), and summing with the difference between the Donnan potentials at the SW and RW interfaces:

$$\Delta\phi_m = \int_0^{d_m} E\, dx + \Delta\phi_D^{SW} - \Delta\phi_D^{RW} \tag{40}$$

Where $\Delta\phi_m$ is the total membrane potential [V], $\Delta\phi_D$ are the Donnan potentials in SW and RW [V], E is the electric field inside the membrane [V/m] and 0 and d_m are the x-coordinates in the membrane of the SW and RW interface, respectively [m].

3.1.4 Discretization

The modeled membrane was discretized into an appropriate number of grid cells so that the desired results were grid size invariant. This depended on the membrane properties. For some simulations less than 10 cells would be sufficient, but to avoid any risks a total of 40 cells was used in most cases. For discretizing the governing equations, second order finite differencing methods were used.

3.2 Nernst uphill transport model

The occurrence of uphill transport in RED results in a significant loss of OCV [14,16,18]. This loss was quantified by calculating the equilibrium OCV through Vermaas' uphill transport model [18]. In Vermaas' model, two monovalent ions are exchanged for one divalent ion until the Nernst potentials of the two species match. For an AEM this means that two Nernst equations for the OCV of chloride and sulfate need to be solved for a concentration change that happens through uphill transport. Neglecting a difference in permselectivity for the two OCVs, we first have the sulfate and chloride voltages:

$$E_{SO_4^{2-}} = \frac{RT}{2 \cdot F} \ln\left(\frac{\gamma_{SO_4^{2-}}^{sw} c_{SO_4^{2-}}^{sw}}{\gamma_{SO_4^{2-}}^{rw} c_{SO_4^{2-}}^{rw}}\right) \tag{41}$$

$$E_{Cl^-} = \frac{RT}{F} \ln\left(\frac{\gamma_{Cl^-}^{sw} c_{Cl^-}^{sw}}{\gamma_{Cl^-}^{rw} c_{Cl^-}^{rw}}\right) \tag{42}$$

With R, T and F their usual meaning and γ and c are the activity coefficient [-] and concentration of the indicated ions in the indicated feedwaters [mol.m^{-3}].

To equilibrate the two voltages, the variable x_{up} is introduced. It represents the amount of sulfate that is moved from RW to SW. A sulfate concentration equal to x_{up} is moved to the seawater and subtracted from the RW. Because the transport must be electroneutral, two chloride ions move in the opposite direction from SW to RW, for each sulfate ion. Consequently, $2x_{up}$ is subtracted from the SW concentration and added to the RW. This results in the following equation for the equilibrium OCV voltage:

$$\left(\frac{\gamma_{SO_4^{2-}}^{sw}(x_{up}) \cdot (c_{SO_4^{2-}}^{sw} + x_{up})}{\gamma_{SO_4^{2-}}^{rw}(x_{up}) \cdot (c_{SO_4^{2-}}^{rw} - x_{up})}\right)^{\frac{1}{2}} = \left(\frac{\gamma_{Cl^-}^{sw}(x_{up}) \cdot (c_{Cl^-}^{sw} - 2x_{up})}{\gamma_{Cl^-}^{rw}(x_{up}) \cdot (c_{Cl^-}^{rw} + 2x_{up})}\right) \tag{43}$$

Where $\gamma(x_{up})$ indicates the dependency of the activity coefficients on the uphill transport concentration change x_{up}.

The equilibrium was solved numerically, through a custom Python function that applied a built-in SciPy root-finding algorithm. The activity coefficients are calculated using the model of Ge et al. [49], which the root-finding function includes in calculating the equilibrium. The change in activity coefficients that comes with a change in composition are therefore included in the solution, unlike the original model by Vermaas, which assumed constant activity coefficients [18].

4 Methods

4.1 Solution method

The steady state model was solved using an algorithm based on the multivariate Newton-Rhapson method. The Newton-Rhapson method is a well-known root-finding method that has a high convergence rate [53].

The Newton-Rhapson algorithm evaluates a function at a certain point and approximates it using the local (numerical) tangent line. A step from the given point to the root of this tangent is calculated and this root is used as the new point for evaluation. This process is iterated until the change between points is below a set tolerance value and the root of the function is found. See **Figure 5** below.

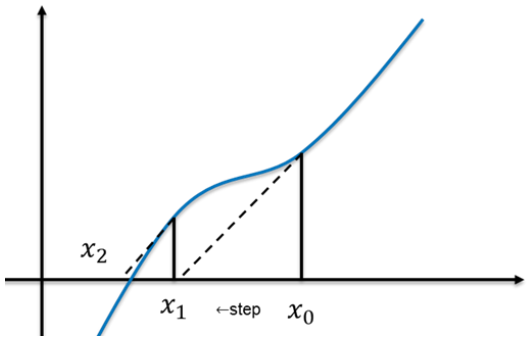

Figure 5. Illustration of the Newton-Rhapson method.

The initial guess for the algorithm is very important [53]. If the initial guess is far off, it may diverge from the actual solution. Luckily, for our model the concentration profiles are very well approximated by straight lines, so the initial guess is good.

The Newton-Rhapson algorithm can be extended to multivariate cases, making use of linear algebra and matrix equations. The model is described by a set of mass balances (the equations) that are a function of the concentrations throughout the membrane (the variables). Instead of one derivate, a Jacobian matrix is constructed containing the partial derivatives to the concentrations for which the model is solved. Just like the one-dimensional case illustrated above, these partial derivatives are used to compute a step change for all concentrations.

Sometimes, the step change that the algorithm calculates may provide negative concentrations. To ensure the system provides only real solutions and prevent errors, a smaller step (step relaxation) is performed when the step is too large.

A flowchart of the membrane model can be found in the appendix.

4.2 Simulations

Both the membrane model and the Nernst uphill transport model were used to show the effect of divalent ions on membrane performance in RED. A choice was made to show only simulations performed for AEMs and limit the presence of multivalent ions to sulfate only, as for those simulations the necessary data for validation and membrane properties was readily available, provided by Pintossi. The simulated conditions are the same as described in the work of Pintossi et al. [14]. Seawater was given a total salt concentration of 508 mM and river water 17mM. For simulation including sulfate, a fraction of the total NaCl salt concentration was replaced by Na_2SO_4. This is in line with the experiments performed by Pintossi et al. whom chose to do this to keep the chloride gradient between feedwaters constant when sulfate was added in equal fractions to both feedwaters [14].

The occurrence of uphill transport as a function of feedwater composition was predicted using the Nernst equation and the membrane model. For both approaches, the molar fractions of sulfate in RW and SW were varied between 0.1% and 50%. Application of Vermaas' uphill transport model identified uphill transport by comparing the Nernst OCVs of sulfate and chloride [18], while for the membrane model, the direction of sulfate flux showed whether uphill transport took place or not. The definition of the flux equation was varied to show if convection influences the appearance of uphill transport.

The effect of sulfate on the apparent permselectivity was investigated using a combination of the membrane model and Vermaas' model. In line with available experimental data, sulfate fractions of 0-25-50% were added to either RW only, SW only, or both. First, the equilibrium OCV and equilibrium composition after uphill transport were calculated using Vermaas' Nernst-based uphill transport model [18]. Afterwards, the equilibrium composition was used as input for the membrane model, to calculate the membrane potential. The apparent permselectivity followed from the ratio of the

membrane potential and the equilibrium OCV. For the membrane potential, two AEM membranes were simulated: Fujifilm type 1 and type 10. The type 1 membrane was used to show the effect of the membrane charge density on the permselectivity, by multiplying the simulated charge density with a factor X_r, varying from 0.2-2.

To show the real potential of the membrane model, a fit was made to the experimental permselectivity data of both membranes. The membrane diffusion coefficients were multiplied with a fitting parameter, in addition to the steric factor in Mackie and Meares' model [38]. The choice for fitting was on the diffusion coefficients because they were the only membrane parameters that were not directly obtained from experimental measurements.

After showing the validity of the model with fit diffusion coefficients, the importance of convective transport on the membrane permselectivity is shown. The membrane simulation with the fitted diffusion coefficient is repeated for the type 1 AEM, but without convective transport included in the flux equation.

5 Results and discussion

5.1 Uphill transport

5.1.1 Nernst equation

The Nernst OCVs of the multivalent and monovalent ions were calculated using the Nernst equation and compared. Following Vermaas' model, uphill transport occurs when the OCV of the monovalent species is higher than the multivalent one, so the difference between the two voltages must be taken. This difference between chloride and sulfate (mono-and divalent, respectively) OCVs is given in **Figure 6**, where the sulfate OCV was subtracted from the chloride OCV. Based on the concentration ratio only, the centered $y = x$ line is expected to be the line where the OCV difference is zero, but this is not the case. For most of the graph, the difference is positive, meaning a higher OCV of chloride. There are two reasons for this phenomenon.

The first reason is obvious, based on the definition of the Nernst equation, equation (26): the valency of the divalent ion also adds a factor $\frac{1}{2}$ to the OCV. The second reason for the higher OCV is that the activity coefficient ratio of monovalent ions is higher than that of divalent ions. The activity of monovalent ions is in generally higher than that of multivalent ions and this effect is more pronounced in seawater because of the higher ionic strength of the solution. The higher the ionic strength of a solution, the more the activity coefficient is lowered, as also stated by the Debye-Hückel theory [54]. In river water, all activity coefficients are higher and less influenced by the valency of the ions because of the lower ionic strength of the solution. This is also reflected by the activity coefficient model by Ge et al. used for this model [49]. See Table 2 for an example of the activity coefficients in both solutions at a molar sulfate fraction of 25%.

Table 2. Approximate activity coefficients of ions in SW an RW, predicted using the TCPC model of Ge et al.[49]**. Sulfate fraction in both waters 25%.**			
Ion species	Cl^-	SO_4^{2-}	Na^+
Activity coefficient SW [-]	0.68	0.37	0.68
Activity coefficient RW [-]	0.87	0.75	0.87

Although for most of the simulated compositions the monovalent OCV is larger, there are is also an area where the OCV of sulfate exceeds that of chloride. In this upper left area of **Figure 6**,we have uphill transport of chloride instead of sulfate, but that area of low RW sulfate fraction and high SW sulfate fraction is outside of natural feedwater conditions (in the Netherlands) [14,18].

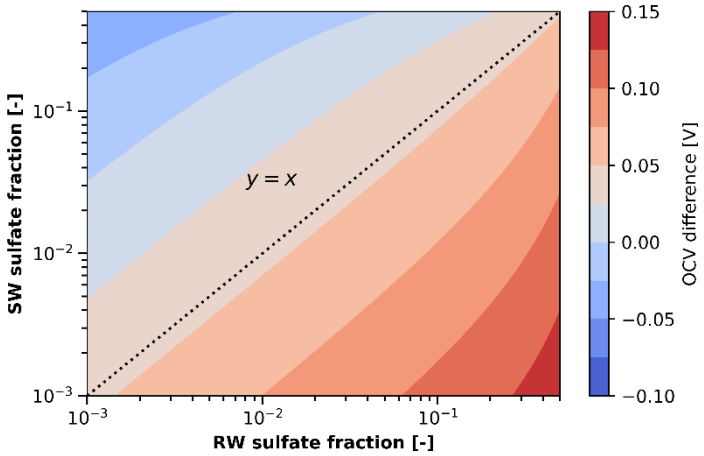

Figure 6. OCV difference for an AEM as a function of composition. Predicted by the Nernst equation. Above the y=x line, the concentration ratio favors sulfate, while below it the concentration ratios favor chloride.

Besides the absolute difference, it is also valuable to look at the relative difference between the two voltages, as this gives a better indication of the relative extent to which uphill transport takes place. The relative difference was calculated by dividing the difference in OCVs between monovalent and divalent species with the maximum value of the two. The result is visible in **Figure 7**.

An interesting region of this graph is where the difference between voltages is (nearly) zero, as this is the region where there is little to no uphill transport and the voltages of sulfate and chloride are

practically equal. This region can be indicated by a line for which the voltages are exactly equal, and the difference is zero. We will call it the Nernst zero-line.

If the solution is ideal and activity coefficients are neglected, the Nernst zero-line can be derived analytically, which gives the ideal Nernst-zero-line. When including activity coefficients, the effect of the difference in activity coefficient ratios for monovalent and multivalent ions becomes visible. Because the ratio of divalent ions is lower than that of monovalent ions, the zero line moves to the top left corner, where the concentration ratio of sulfate increases and the ratio of chloride lowers. Both lines can be seen in **Figure 7**, along with the relative OCV difference.

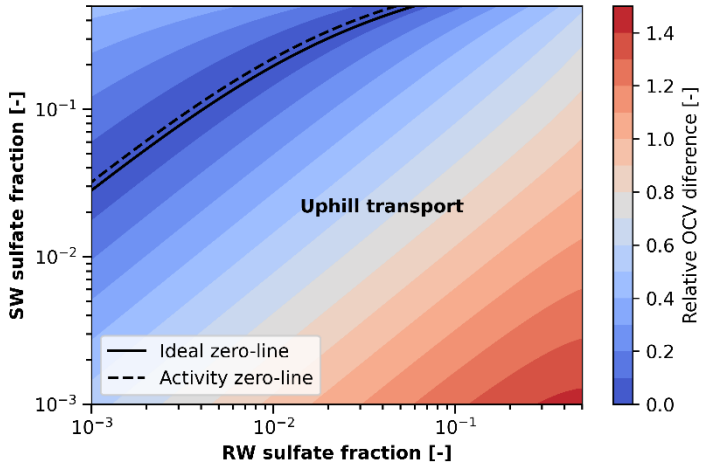

Figure 7. Relative OCV difference between sulfate and chloride. Calculated using the Nernst equation including activity coefficients. Zero-lines indicate where the chloride and sulfate OCV are equal and the difference is zero.

5.1.2 Membrane model

The occurrence of uphill transport at OCV conditions is much more straightforward in the membrane model. The direction of flux is defined from the seawater towards the river water. This means that if the flux calculated by the model is positive, we have transport from high concentration to low concentration, 'downhill' transport. When the flux is negative, we do have uphill transport.

The steady state flux at OCV conditions was calculated for two simulated anion exchange membranes, Fujifilm AEM type 1 and Fujifilm AEM type 10. The relevant properties of the two membranes are given in .

Table 3.

Table 3. Fujifilm AEM type 1 and 10 membrane properties.

Membrane	Thickness (μm)	Charge density (mol. eq./m^3)	Water permeability (m^3/m^{2}bar.s)	Water volume fraction (-)
Type 1	120	1650	$1.809 \cdot 10^{-9}$	0.53
Type 10	120	2850	$4.175 \cdot 10^{-9}$	0.38

The flux equation used was varied for both membrane types. Both the regular (no convection) and extended NP equation were used to see the influence of the modelling method on the zero-lines. Two variations of the convection term in the extended NP equation were employed: one with only an osmotic pressure gradient and one with both a pressure gradient and the electric field. Interestingly, as visible in **Figure 8**, the definition of the flux equation does not change the location of the zero-line.

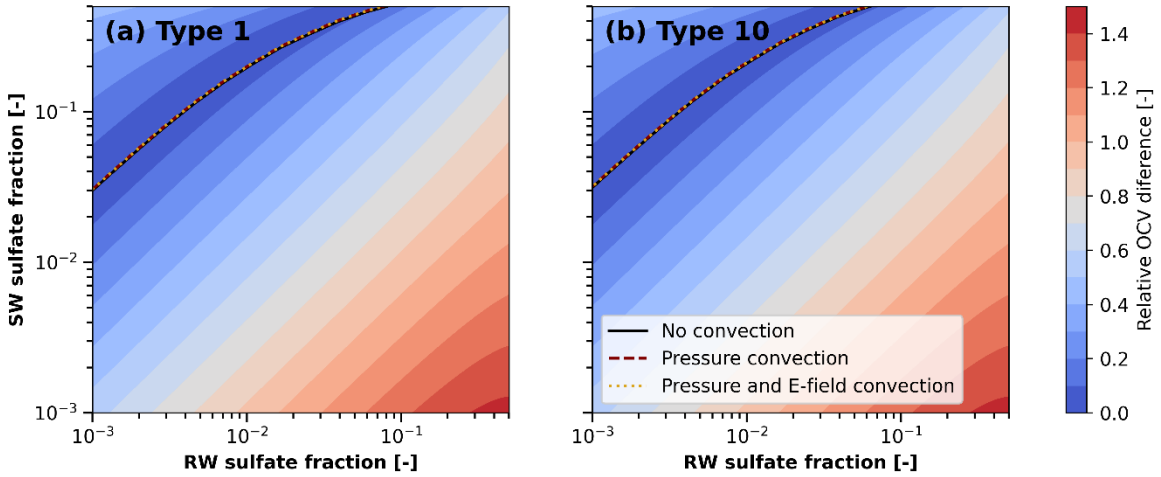

Figure 8. Zero-lines as a function of SW and RW composition. (a) Fujifilm AEM type 1 and (b) Fujifilm AEM type 10 membranes. Three different definitions of the Nernst-Planck flux equation were used: without convection, convection based on the osmotic pressure difference and convection based on a combination of osmotic pressure and the electric field. The position of the zero-lines is independent of the definition of the flux.

The conclusion can be drawn that including convective transport in the NP flux equation does not significantly influence whether uphill transport occurs. It should be noted, however, that these two membranes only cover a very small range of water permeability coefficients. However, the main

reason for uphill transport is the Donnan exclusion effect caused by the membrane charge density, because the Donnan equilibrium determines the concentration of the membrane. Combined with the fact that for RED membranes the water permeability is low in general, the effect of convection on the occurrence of uphill transport is expected to be low as well.

The comparison between the Nernst equation and the membrane model can be seen in **Figure 9**. The two models show good agreement on when uphill transport is expected to occur, with only a small deviation for the membranes at higher sulfate fractions. The type 1 membrane shows a slightly lower zero-line that can be attributed to the lower charge density than the type 10 membrane. The reason for this is the lower the Donnan exclusion effect, which results in less pronounced uphill transport. This is illustrated by lowering the membrane charge density (X_M) of a type 1 membrane to a fraction of 0.25 times its original membrane charge density (1.65M).

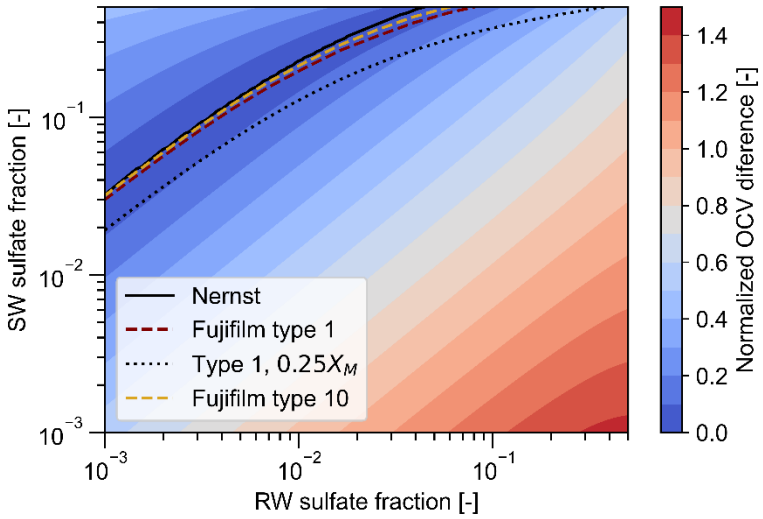

Figure 9. Comparison of Nernst zero-line with Fujifilm type 1 and 10 membrane simulations. The Nernst equation and membrane models show good agreement, if the charge density in the membrane is high enough. If the charge density is lowered, as indicated by the dotted line for the type 1 membrane, the zero line moves to lower sulfate fractions.

To investigate and predict permselectivity data, it is important that the membrane model and Nernst equation agree that there is no net transport across the membrane under OCV conditions if the two are compared for a given feedwater composition. If either one of the models is not at or near equilibrium for those feedwater concentrations, it does not make much sense to look at the

permselectivity there. Fortunately, **Figure 9** shows good agreement between Nernst and membrane model, for both membrane types. It is therefore assumed that the two models can be used together.

5.1.3 OCV loss through uphill transport

When predicting the apparent permselectivity of the membrane, knowledge of the theoretical potential is required. The Nernst equation is used for the theoretical potential of mixtures containing a single valency, but for a given composition of a multi-ionic mixture, the theoretical voltage can have multiple values. Therefore, something like Vermaas' model of uphill transport must be used to obtain the theoretical potential [18]. This provides the equilibrium potential where the di-and monovalent potentials are the same and uphill transport is accounted for. The effect of the presence of sulfate on this equilibrium OCV through uphill transport is shown in **Figure 10**, where sulfate was added to either RW, SW or both feedwaters.

Adding a fraction of sulfate to RW means adding only a little sulfate to the system, compared to adding the same fraction in SW. However, the normalized OCV is not much higher than adding sulfate to the SW, especially at low fractions. The equilibrium OCV is relatively sensitive to the concentration in RW, but in the end the total amount of sulfate present in both feedwaters will determine the OCV.

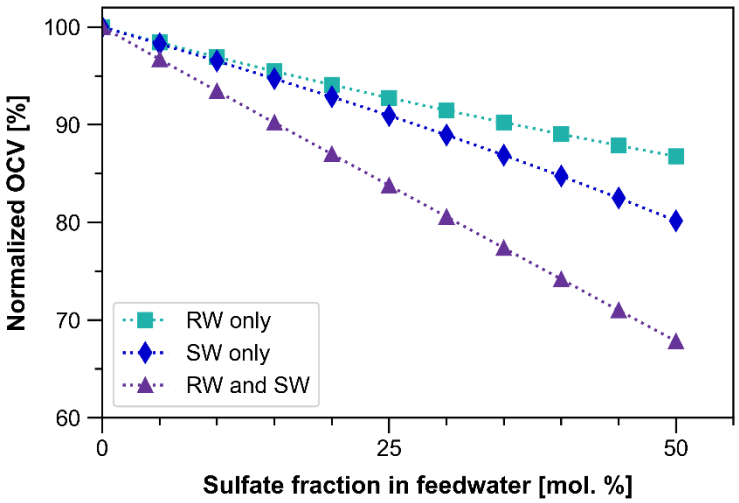

Figure 10. Effect of sulfate fraction in feedwaters on the OCV. Normalized to the OCV without sulfate (87mV). Equilibrium OCV calculated after uphill transport using the model by Vermaas et al. [14].

5.2 Permselectivity

5.2.1 Feedwater composition

Given the calculated feedwater compositions at OCV equilibrium, the membrane model was used to predict the membrane potential under OCV conditions and obtain the apparent permselectivity. Recalling the definition of the apparent permselectivity in equation (29) and use the simulated membrane potential instead of the experimentally measured voltage:

$$\alpha = \frac{\Delta\phi_m}{V_{th}}$$

Where α is the permselectivity [-], $\Delta\phi_m$ is the membrane potential [V] and V_{th} the theoretical Nernst equilibrium voltage [V].

Figure 11 shows the predicted membrane permselectivities from the membrane model as a function of sulfate fraction in SW, RW or both. From this graph, it can be noticed that the permselectivity is less easily influenced by a low amount of sulfate compared to the OCV (RW only case). Increasing the total amount of sulfate in both feedwaters will have a detrimental effect on permselectivity. A higher permselectivity is observed for the membrane type 10, with a lower water permeability and a higher charge density.

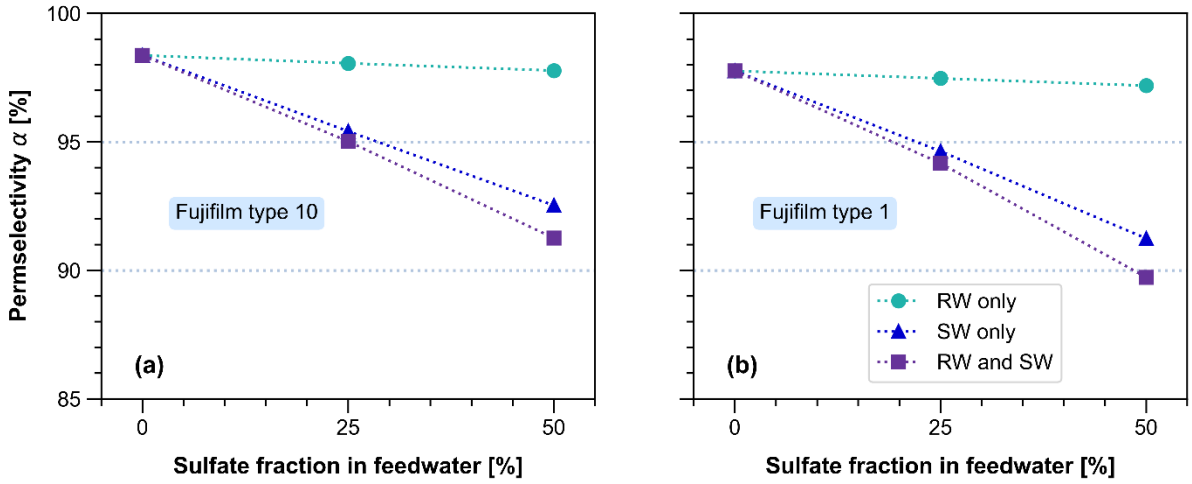

Figure 11. Permselectivity predictions as a function of feedwater composition. (a) Fujifilm AEM type 10 and (b) Fujifilm AEM type 1. Permselectivity is significantly lower at higher sulfate fractions.

5.2.2 Charge density

The permselectivity predicted by the model has a high dependency on the charge density, as shown in **Figure 12**. This is in line with real-world expectations, as a higher charge density has a more pronounced Donnan exclusion effect. The model can therefore potentially be used to predict the effect of 'poisoning' on the membranes, where the effective charge density in the membrane is lowered by the binding of multivalent ions. Also, it underlines the importance of high charge density for better membrane performance in terms of OCV and permselectivity, as shown in previous work [16].

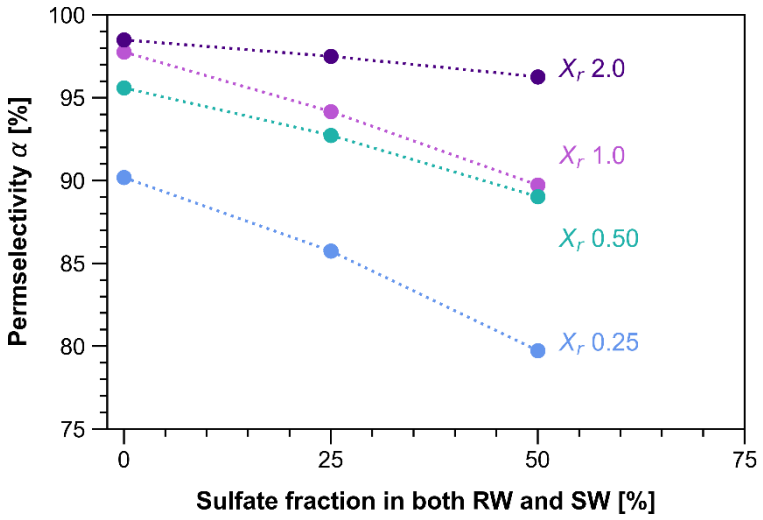

Figure 12. Permselectivity as function of the relative membrane charge density $X_r = X/X_{og}$. Original membrane properties of the Fujifilm AEM type 1 membrane were used.

5.2.3 Experimental fit

The model shows desired behavior, when looking at charge density and feedwater composition. However, without any fitting parameters it was unable to predict the experimentally observed permselectivities. So, one fitting parameter was added to see if including that could improve the membrane model and increase its potential for application in a larger, full scale RED model. **Figure 13** shows that with a single fitting parameter for the diffusion coefficients, the most uncertain parameter for the membranes, the experimental permselectivities can be closely approximated. What effects exactly are captured by this fitting parameter is uncertain, but it greatly improves the performance of the model. Although it is not fully predictive based on model input only, one can use a few experimental OCV measurements to calibrate the model and then use the model to calculate permselectivities for a wider range, without having to perform measurements for all feedwater compositions.

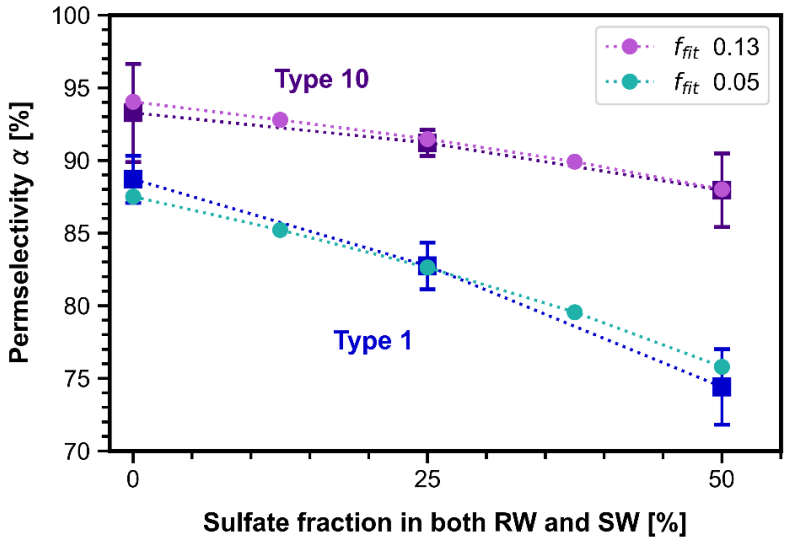

Figure 13. Predicted permselectivity data using fit diffusion coefficients. Both membrane simulations show that with a simple fitting of the diffusion coefficient, the experimental results can be matched closely. Experimental results are plotted using squares and included 95% confidence intervals for measurements.

There are several reasons that could explain the discrepancy between the model and the experimental data without fitting. Not all of them are covered here as they have been mentioned before in the description of the model or the discussion of theory, or they are inherent uncertainties obtained from experimental measurements. Instead, the focus will be on two parts of the modelling strategy that

leave very clear room for improvement: the membrane activity coefficients and the calculation of equilibrium after uphill transport through Vermaas' model.

First, the membrane activity coefficients are assumed to be unity, which neglects any non-ideal behavior inside the membrane. May not be valid, since especially at low external solution concentrations, the strong attraction between fixed charges in the membrane and the ions in solution is expected to generate strong non-ideal behavior [52,55].

Secondly, a disparity between experimental data and model simulations may arise because the mechanism of uphill transport is modelled using Vermaas' model. This model has the underlying assumption that uphill transport is ideal, without co-ion leakage. Vermaas' uphill transport model assumes a fully permselective membrane that only transport counter-ions. This means that the equilibrium composition calculated using Vermaas' model is the most ideal composition, with the maximum theoretical potential after uphill transport, but possibly not the real one.

In reality, there could also be some co-ion leakage from SW to RW during uphill transport. This results in a different equilibrium position with a lower potential than the one given by Vermaas' model. The reason for this lower potential being a larger number of (co-)ions in the RW compartment. It will decrease the effect of Donnan exclusion and hence, the Donnan potential. When Vermaas' equilibrium composition is used as input to the membrane model, the membrane model might overpredict the measured permselectivity because it uses a feedwater composition as input that will have an expected higher permselectivity value compared to what might be the 'real' composition might be during experimental measurement. Unfortunately, no experimental data of the concentrations after uphill transport was present, so this theory will have to be tested still.

It is important to note that the effect of co-ion leakage may be overestimated here, especially when looking at the work by Kingsbury and Coronell [30]. They performed similar research predicting membrane permselectivity, but in absence of multivalent ions. They observed negligible changes between the concentration of ions in their solutions before and after permselectivity measurements for their membranes [30]. This observation opposes the theory for ion leakage. However, the used

membranes were of much higher charge density (>7M) compared to the membranes covered in this work. For such highly charged membranes, a larger effect of Donnan exclusion and less ion leakage is expected. Also, because their work did not cover multivalent ions, there was no influence of uphill transport.

To see how the membrane model would perform with such a highly charged membrane and without multivalent ions, the model was also compared to experimental permselectivities for one of the membranes from the work of Kingsbury and Coronell [30]. Without the need for a fitting parameter, good predictions for the experimental data could be given. This comparison provides confidence in the value of the modelling approach and underlines the importance of investigating non-ideal uphill transport. The comparison can be found in appendix B.

5.2.4 Convection

Convective transport is often neglected in simulation of IEMs [28]. This assumption is based on the fact that the water permeability of IEMs is usually as low as possible, because the only desired transport is that of (counter-)ions. Real membranes have some water permeability and in RED a high osmotic pressure gradient is usually present in the membrane. Kingsbury and Coronell provided an expression for the convective transport through the membrane [30], which greatly improves the performance of the membrane model for this work. The improved performance is illustrated by leaving out the convective term from the flux equation, for which the results are shown in **Figure 14**. The same fit factor as in **Figure 13** was used, yet the permselectivities are far off from the experimental data. Based on these results, a strong recommendation is made to not neglect convective transport in RED membrane modelling.

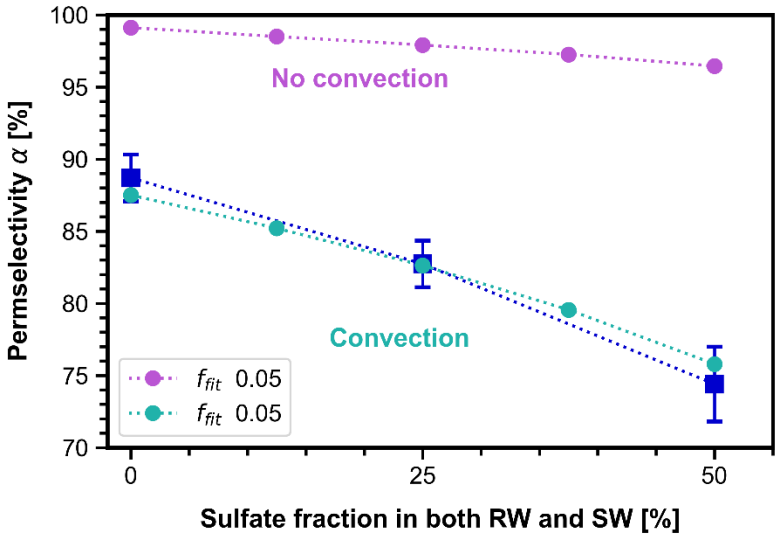

Figure 14. Permselectivity predictions with and without convective transport. The same fitting factor was used as for the permselectivity simulations including convection. Similar to the results shown by Kingsbury and Coronell for monovalent ions [30], the convection through the membrane greatly improves the membrane performance.

6 Conclusion

A steady-state one-dimensional model was created for the modelling of ion exchange membranes for RED applications in the presence of both divalent ions. The modelling approach was based on the Nernst-Planck equation and Donnan-electroneutrality approach. Activity coefficients inside the feedwaters were accounted for, as well as water transport through the membrane. The occurrence of uphill transport within the membrane model was compared to the Nernst-based model by Vermaas and found good agreement [18].

The model was used to predict the apparent permselectivity of two AEMs, Fujifilm type 1 and Fujifilm type 10, in the presence of the divalent sulfate ion. Vermaas' model was used to calculate the equilibrium composition and theoretical OCV after uphill transport and the membrane model used it as input to predict the permselectivity of the AEMs. The positive dependence of permselectivity on membrane charge density was showcased, as well as the importance of including convective transport in the definition of the NP flux equation.

Good agreement was found with experimental data when a single fitting factor was applied to the diffusion coefficients. Two possible causes for discrepancies between the model without fitting factor and the experimental results are discussed: the activity coefficients in the membrane and the assumption of ideal uphill transport, upon which Vermaas' model is built.

The importance of convection is highlighted, further strengthening the notion of Kingsbury and Coronell that the inclusion of convective transport through the membrane improves model performance.

7 Future work

The model described in this work shows good promise for the prediction of membrane permselectivities in the presence of multivalent ions, making it a good starting point for future work. There are possibilities for expanding the model, refining or improving the model, and even model application through integration in larger (multi-)scale models which make use of the Nernst equation. First, refining the model by including the prediction of non-unity membrane activity coefficients is something which can be investigated in future work. Various works by Kamcev et al. have been published in recent years detailing ways to predict activity coefficients in ion exchange membranes using Manning's counterion condensation theory [37,51,52,56]. The recent work of Kingsbury and Coronell included Manning's counterion condensation theory for the prediction of IEM permselectivity, but refrained from including multivalent ions. Therefore, although Kingsbury and Coronell found experimental results to agree better when the condensation theory was ignored and an 'ideal' membrane was considered [30], the lack of multivalent ions still suggest further research into Manning's theory. Especially given the good agreement for membrane activity coefficients found by Kamcev et al. [51].

Secondly, Manning's theory can also be used to improve the theoretical guess of the membrane diffusion coefficients, see the work of Kamcev et al. [37]. Besides the applied Mackie and Meares model with its steric coefficient, they include an electric contribution to the hindered transport through the membrane. Diffusion coefficients in the membrane would then be calculated as follows:

$$D_m = f_{steric} f_{electric} \cdot D_s \tag{44}$$

The electric factors reported by Kamcev et al. for a $MgCl_2$ solution were 0.85 or higher [37]. This means that the permselectivities based on theoretical predictions will be lower when including the electric effect on the diffusion coefficient, closer to the experimental value. In comparison, the fit factors for the type 10 and type 1 membrane were 0.13 and 0.05, respectively. Hence it is doubtful that including Manning's theory for diffusion coefficients will be enough to produce a fully predictive permselectivity

model that matches the experimental results. Instead it is likely that a fully predictive model will require the inclusion of dynamic, non-ideal behavior for determining the membrane potential.

The third possibility for future work lies in adapting the membrane model to predict the transient uphill transport and the equilibrium composition including non-ideal effects.

Fourth, expanding the model to a full RED cell is also an interesting option (even without improvements). To the best of our knowledge there is no modelling work yet on the performance of a full RED cell including multivalent ions. Expanding the model and using it for optimization of the full RED cell can be valuable to RED development.

Lastly, besides model improvements or expansion, the model in its current form can be used to predict permselectivities and membrane resistances of membranes depending on the feedwater composition. Although the author acknowledges the fact that he has little knowledge of the state of RED upscaling and optimization for real-world applications, the model can be useful for modelling and optimization of RED on a larger scale. Numerous (multiscale) models reported in literature make use of the Nernst equation for predicting the power density of RED, for example the multiscale CFD [13,23,57]. The 1D membrane model can be used in those types of models to allow them to adapt to more realistic feedwaters, including multivalent ions. It can be used to predict permselectivities and uphill transport as a function of feedwater composition, instead of treating the permselectivity as a constant.

8 Acknowledgement

A word of thanks

Almost exactly a year from when I started, I have finished my journey to finish the work you have read just now. And what a journey it was. Through a global pandemic crisis, two lockdowns, many, many, silly mistakes and a hard-to-ease critical mindset that more often hurt me than helped me, I have finished it. But, of course, I could not have gotten here by myself. I am hugely grateful for all the support, help and kindness I have been given by everyone who helped me get here.

First, I thank my supervisor Diego. I cannot express in words how nice it was to have you support me, trust in me and show me kindness when I was only hard on myself. Thank you for our many digital conversations, always being helpful, reachable and for trusting in me when we went on a totally different journey than we initially imagined. I would have loved to be able to work together in real life, I wish you best of luck with the final stretch of your PhD.

Thanks to Kitty and Caroline for their advice when the going got tough, and always being there to provide a listening ear. You did everything you could to make me feel welcome in the group. Even when right after I joined, covid-19 was making it harder than ever to have that group-feeling that brought me to MM/P in the first place. Kind thanks to the committee members Kay and Zandrie also, for providing me with feedback halfway through the year.

Lastly, a thanks to my friends Hendrik and Adam. Adam, you provided me with a workspace when I most needed to get out of my room. Hendrik, thank you for staring with me at my whiteboard when I was trying to solve a problem and needed a listening ear, thank you for your advice and thoughts and thank you for surviving the lockdowns with me.

9 Bibliography

[1] International Energy Agency, World Energy Outlook 2015, 2015. www.iea.org/t&c (accessed April 30, 2018).

[2] J.W. Post, J. Veerman, H.V.M. Hamelers, G.J.W. Euverink, S.J. Metz, K. Nymeijer, C.J.N. Buisman, Salinity-gradient power: Evaluation of pressure-retarded osmosis and reverse electrodialysis, J. Memb. Sci. 288 (2007) 218–230. doi:10.1038/s41545-020-0073-7.

[3] O.A. Alvarez-Silva, A.F. Osorio, C. Winter, Practical global salinity gradient energy potential, Renew. Sustain. Energy Rev. 60 (2016) 1387–1395. doi:10.1016/J.RSER.2016.03.021.

[4] M. Tedesco, A. Cipollina, A. Tamburini, G. Micale, Towards 1 kW power production in a reverse electrodialysis pilot plant with saline waters and concentrated brines, J. Memb. Sci. 522 (2017) 226–236. doi:10.1016/j.memsci.2016.09.015.

[5] N.Y. Yip, D. Brogioli, H.V.M. Hamelers, K. Nijmeijer, Salinity gradients for sustainable energy: Primer, progress, and prospects, Environ. Sci. Technol. 50 (2016) 12072–12094. doi:10.1021/acs.est.6b03448.

[6] R.A. Tufa, S. Pawlowski, J. Veerman, K. Bouzek, E. Fontananova, G. di Profio, S. Velizarov, J. Goulão Crespo, K. Nijmeijer, E. Curcio, Progress and prospects in reverse electrodialysis for salinity gradient energy conversion and storage, Appl. Energy. 225 (2018) 290–331. doi:10.1016/j.apenergy.2018.04.111.

[7] R.R. Gonzales, A. Abdel-Wahab, S. Adham, D.S. Han, S. Phuntsho, W. Suwaileh, N. Hilal, H.K. Shon, Salinity gradient energy generation by pressure retarded osmosis: A review, Desalination. 500 (2021) 114841. doi:10.1016/j.desal.2020.114841.

[8] G. Manecke, Membranakkumulator, Zeitschrift Für Phys. Chemie. 201 (1952). doi:10.1515/zpch-1952-20102.

[9] R.E. Pattle, Production of electric power by mixing fresh and salt water in the hydroelectric pile, Nature. 174 (1954) 660. https://link.springer.com/content/pdf/10.1038/174660a0.pdf (accessed July 21, 2020).

[10] A. Cipollina, G. Micale, A. Tamburini, M. Tedesco, L. Gurreri, J. Veerman, S. Grasman, Reverse electrodialysis: Applications, in: Sustain. Energy from Salin. Gradients, Woodhead Publishing, 2016: pp. 135–180. doi:10.1016/B978-0-08-100312-1.00005-5.

[11] F.G. Donnan, The theory of membrane equilibria, Chem. Rev. 1 (1924) 73–90. doi:10.1021/cr60001a003.

[12] D.A. Vermaas, J. Veerman, N.Y. Yip, M. Elimelech, M. Saakes, K. Nijmeijer, High Efficiency in Energy Generation from Salinity Gradients with Reverse Electrodialysis, ACS Sustain. Chem. Eng. 1 (2013) 1295–1302. doi:10.1021/sc400150w.

[13] C. Simões, D. Pintossi, M. Saakes, Z. Borneman, W. Brilman, K. Nijmeijer, Electrode segmentation in reverse electrodialysis: Improved power and energy efficiency, Desalination. 492 (2020) 114604. doi:10.1016/j.desal.2020.114604.

[14] D. Pintossi, C.-L. Chen, M. Saakes, K. Nijmeijer, Z. Borneman, Influence of sulfate on anion exchange membranes in reverse electrodialysis, NPJ Clean Water. 3 (2020) 29. doi:10.1038/s41545-020-0073-7.

[15] B. Tansel, Significance of thermodynamic and physical characteristics on permeation of ions during membrane separation: Hydrated radius, hydration free energy and viscous effects, Sep. Purif. Technol. 86 (2012) 119–126. doi:10.1016/j.seppur.2011.10.033.

[16] A.A. Moya, Uphill transport in improved reverse electrodialysis by removal of divalent cations in the dilute solution: A Nernst-Planck based study, J. Memb. Sci. 598 (2020) 117784. doi:10.1016/j.memsci.2019.117784.

[17] T. Rijnaarts, E. Huerta, W. Van Baak, K. Nijmeijer, Effect of Divalent Cations on RED Performance and Cation Exchange Membrane Selection to Enhance Power Densities, Environ. Sci. Technol. 51 (2017) 13028–13035. doi:10.1021/acs.est.7b03858.

[18] D.A. Vermaas, J. Veerman, M. Saakes, K. Nijmeijer, Influence of multivalent ions on renewable energy generation in reverse electrodialysis, Energy Environ. Sci. 7 (2014) 1434–1445. doi:10.1039/C3EE43501F.

[19] A.A. Moya, A Nernst-Planck analysis on the contributions of the ionic transport in permeable ion-exchange membranes to the open circuit voltage and the membrane resistance in reverse electrodialysis stacks, (2017). doi:10.1016/j.electacta.2017.04.022.

[20] Y. Lanteri, A. Szymczyk, P. Fievet, Membrane potential in multi-ionic mixtures, J. Phys. Chem. B. 113 (2009) 9197–9204. doi:10.1021/jp901110c.

[21] J.A. Manzanares, W.D. Murphy, S. Mafé, H. Reiss, Numerical Simulation of the Nonequilibrium Diffuse Double Layer in Ion-Exchange Membranes, 1993. https://pubs.acs.org/sharingguidelines (accessed June 14, 2020).

[22] V. Nikonenko, V. Zabolotsky, C. Larchet, B. Auclair, G. Pourcelly, Mathematical description of ion transport in membrane systems, Desalination. 147 (2002) 369–374. doi:10.1016/S0011-9164(02)00611-2.

[23] M. Tedesco, A. Cipollina, A. Tamburini, I.D.L. Bogle, G. Micale, A simulation tool for analysis and design of reverse electrodialysis using concentrated brines, Chem. Eng. Res. Des. 93 (2015) 441–456. doi:10.1016/j.cherd.2014.05.009.

[24] J. Veerman, M. Saakes, S.J. Metz, G.J. Harmsen, Reverse electrodialysis: A validated process model for design and optimization, Chem. Eng. J. 166 (2011) 256–268. doi:10.1016/j.cej.2010.10.071.

[25] J. Gi Hong, W. Zhang, J. Luo, Y. Chen, Modeling of power generation from the mixing of simulated saline and freshwater with a reverse electrodialysis system: The effect of monovalent and multivalent ions, (2013). doi:10.1016/j.apenergy.2013.04.015.

[26] A.H. Galama, J.W. Post, H.V.M. Hamelers, V. V. Nikonenko, P.M. Biesheuvel, On the origin of the membrane potential arising across densely charged ion exchange membranes: How well does the teorell-meyer-sievers theory work?, J. Membr. Sci. Res. 2 (2016) 128–140. doi:10.22079/jmsr.2016.20311.

[27] A.A. Moya, Theory of the formation of the electric double layer at the ion exchange membrane-solution interface, Phys. Chem. Chem. Phys. 17 (2015) 5207–5218. doi:10.1039/c4cp05702c.

[28] M. Tedesco, H.V.M. Hamelers, P.M. Biesheuvel, Nernst-Planck transport theory for (reverse) electrodialysis: I. Effect of co-ion transport through the membranes, J. Memb. Sci. 510 (2016) 370–381. doi:10.1016/j.memsci.2016.03.012.

[29] H. Fan, N.Y. Yip, Elucidating conductivity-permselectivity tradeoffs in electrodialysis and reverse electrodialysis by structure-property analysis of ion-exchange membranes, J. Memb. Sci. 573 (2019) 668–681. doi:10.1016/j.memsci.2018.11.045.

[30] R.S. Kingsbury, O. Coronell, Modeling and validation of concentration dependence of ion exchange membrane permselectivity: Significance of convection and Manning's counter-ion condensation theory, J. Memb. Sci. (2020) 118411. doi:10.1016/j.memsci.2020.118411.

[31] M. Tedesco, H.V.M. Hamelers, P.M. Biesheuvel, Nernst-Planck transport theory for (reverse) electrodialysis: II. Effect of water transport through ion-exchange membranes, J. Memb. Sci. 531 (2017) 172–182. doi:10.1016/j.memsci.2017.02.031.

[32] M. Tedesco, H.V.M. Hamelers, P.M. Biesheuvel, Nernst-Planck transport theory for (reverse) electrodialysis: III. Optimal membrane thickness for enhanced process performance, J. Memb. Sci. 565 (2018) 480–487. doi:10.1016/j.memsci.2018.07.090.

[33] S. Moshtarikhah, N.A.W. Oppers, M.T. de Groot, J.T.F. Keurentjes, J.C. Schouten, J. van der Schaaf, Nernst–Planck modeling of multicomponent ion transport in a Nafion membrane at high current density, J. Appl. Electrochem. 47 (2017) 51–62. doi:10.1007/s10800-016-1017-2.

[34] S. Honarparvar, D. Reible, Modeling multicomponent ion transport to investigate selective ion removal in electrodialysis, Environ. Sci. Ecotechnology. 1 (2020) 100007. doi:10.1016/j.ese.2019.100007.

[35] M. Tedesco, C. Scalici, D. Vaccari, A. Cipollina, A. Tamburini, G. Micale, Performance of the first reverse electrodialysis pilot plant for power production from saline waters and concentrated brines, J. Memb. Sci. 500 (2016) 33–45. doi:10.1016/j.memsci.2015.10.057.

[36] H. Strathmann, Ion-exchange membrane separation processes, 1st ed., Elsevier, Amsterdam; Boston, 2004.

[37] J. Kamcev, D.R. Paul, G.S. Manning, B.D. Freeman, Predicting salt permeability coefficients in highly swollen, highly charged ion exchange membranes, ACS Appl. Mater. Interfaces. 9 (2017) 4044–4056. doi:10.1021/acsami.6b14902.

[38] J.S. Mackie, P. Meares, The Diffusion of Electrolytes in a Cation-Exchange Resin Membrane. I. Theoretical, Proc. R. Soc. Lond. A. Math. Phys. Sci. 232 (1955) 489–509. www.jstor.org/stable/99826 (accessed February 22, 2021).

[39] P.M. Biesheuvel, Two-fluid model for the simultaneous flow of colloids and fluids in porous media, J. Colloid Interface Sci. 355 (2011) 389–395. doi:10.1016/j.jcis.2010.12.006.

[40] A.E. Yaroschchuk, Transport properties of long straight nano-channels in electrolyte solutions: A systematic approach, Adv. Colloid Interface Sci. 168 (2011) 278–291. doi:10.1016/j.cis.2011.03.009.

[41] Y. Lanteri, P. Fievet, A. Szymczyk, Evaluation of the steric, electric, and dielectric exclusion model on the basis of salt rejection rate and membrane potential measurements, J. Colloid Interface Sci. 331 (2009) 148–155. doi:10.1016/j.jcis.2008.11.014.

[42] P. Fievet, M. Sbaï, A. Szymczyk, Analysis of the pressure-induced potential arising across selective multilayer membranes, J. Memb. Sci. 264 (2005) 1–12. doi:10.1016/j.memsci.2005.04.011.

[43] S. Déon, A. Escoda, P. Fievet, P. Dutournié, P. Bourseau, How to use a multi-ionic transport model to fully predict rejection of mineral salts by nanofiltration membranes, Chem. Eng. J. 189 (2012) 24–31. doi:10.1016/j.cej.2012.02.014.

[44] M. Valiskó, D. Boda, The effect of concentration- and temperature-dependent dielectric constant on the activity coefficient of NaCl electrolyte solutions, J. Chem. Phys. 140 (2014) 234508. doi:10.1063/1.4883742.

[45] A.W. Mohammad, Y.H. Teow, W.L. Ang, Y.T. Chung, D.L. Oatley-Radcliffe, N. Hilal, Nanofiltration membranes review: Recent advances and future prospects, Desalination. 356 (2015) 226–254. doi:10.1016/j.desal.2014.10.043.

[46] D.A. Vermaas, D. Kunteng, M. Saakes, K. Nijmeijer, Fouling in reverse electrodialysis under natural conditions, Water Res. 47 (2013) 1289–1298. doi:10.1016/j.watres.2012.11.053.

[47] J.W. Post, H.V.M. Hamelers, C.J.N. Buisman, Influence of multivalent ions on power production from mixing salt and fresh water with a reverse electrodialysis system, J. Memb. Sci. 330 (2009) 65–72. doi:10.1016/j.memsci.2008.12.042.

[48] F. Gagnon, D. Ziegler, M. Fafard, D. Ziegler, Electrochemical modelling using electroneutrality equation as a constraint, J Appl Electrochem. 44 (2014) 361–381. doi:10.1007/s10800-014-0662-6.

[49] X. Ge, X. Wang, M. Zhang, S. Seetharaman, Correlation and prediction of activity and osmotic coefficients of aqueous electrolytes at 298.15 K by the modified TCPC model, J. Chem. Eng. Data. 52 (2007) 538–547. doi:10.1021/je060451k.

[50] M.-T. Hsieh, S.-T. Lin, A predictive model for the excess gibbs free energy of fully dissociated electrolyte solutions, AIChE J. 57 (2011) 1061–1074. doi:10.1002/aic.12325.

[51] J. Kamcev, D.R. Paul, B.D. Freeman, Ion Activity Coefficients in Ion Exchange Polymers: Applicability of Manning's Counterion Condensation Theory, Macromolecules. 48 (2015) 8011–8024. doi:10.1021/acs.macromol.5b01654.

[52] J. Kamcev, M. Galizia, F.M. Benedetti, E.S. Jang, D.R. Paul, B.D. Freeman, G.S. Manning, Partitioning of mobile ions between ion exchange polymers and aqueous salt solutions: Importance of counter-ion condensation, Phys. Chem. Chem. Phys. 18 (2016) 6021–6031. doi:10.1039/c5cp06747b.

[53] W.H. Press, S.A. Teukolsky, W.T. Vetterling, B.P. Flannery, Numerical recipes: the art of scientific computing, Third, Cambridge University Press, Cambridge, 2007.

[54] G.M. Kontogeorgis, B. Maribo-Mogensen, K. Thomsen, The Debye-Hückel theory and its importance in modeling electrolyte solutions, (2018). doi:10.1016/j.fluid.2018.01.004.

[55] M. Galizia, G.S. Manning, D.R. Paul, B.D. Freeman, Ion partitioning between brines and ion exchange polymers, Polymer (Guildf). 165 (2019) 91–100. doi:10.1016/j.polymer.2019.01.026.

[56] J. Kamcev, D.R. Paul, G.S. Manning, B.D. Freeman, Accounting for frame of reference and thermodynamic non-idealities when calculating salt diffusion coefficients in ion exchange membranes, J. Memb. Sci. 537 (2017) 396–406. doi:10.1016/j.memsci.2017.05.034.

[57] Z. Jalili, O.S. Burheim, K.E. Einarsrud, Computational Fluid Dynamics Modeling of the Resistivity and Power Density in Reverse Electrodialysis: A Parametric Study, Membranes (Basel). 10 (2020) 209. doi:10.3390/membranes10090209.

Appendix A. Model flowchart

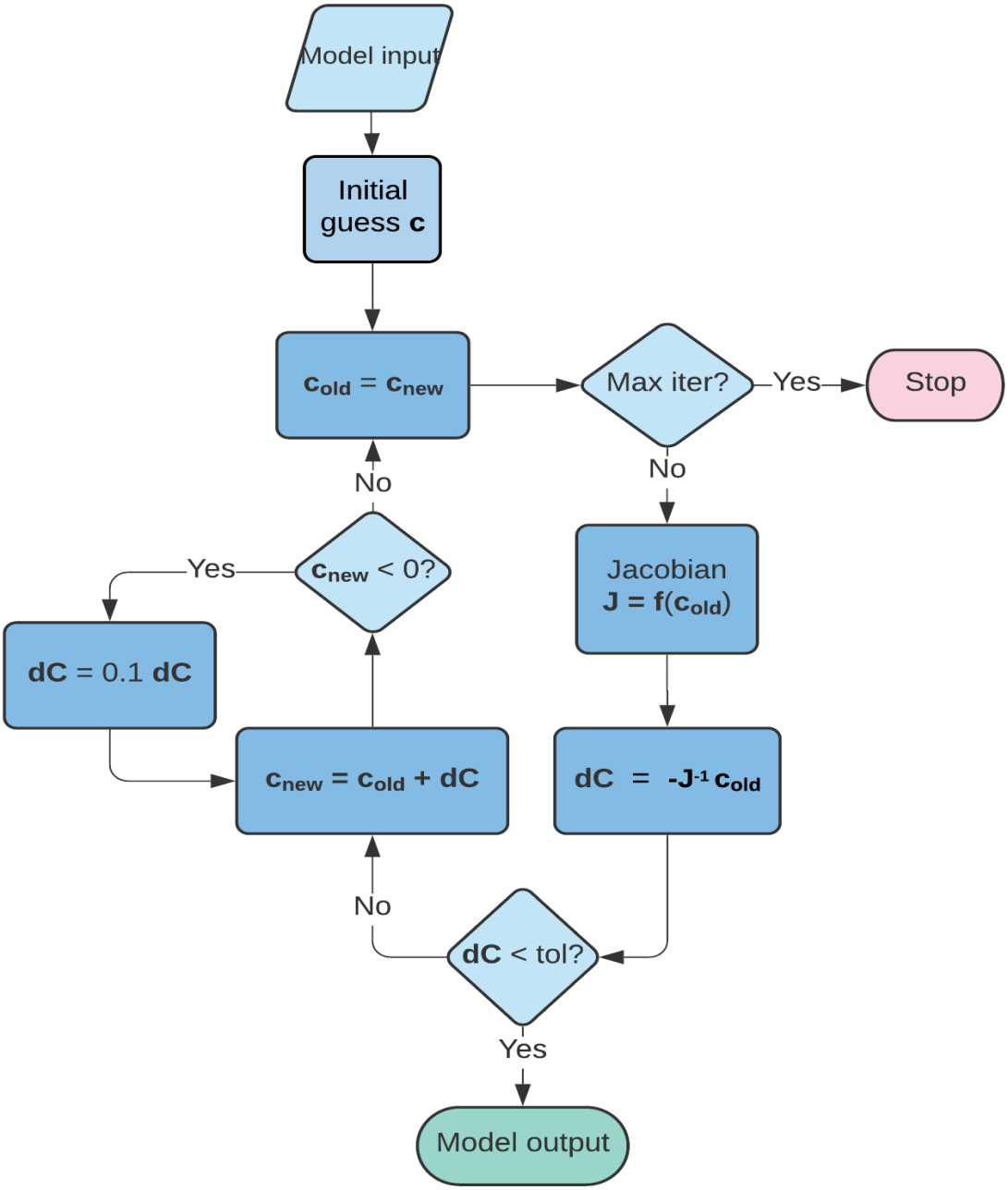

Appendix B: Model comparison for NaCl

The membrane model was validated against one of the membranes reported by Kingsbury and Coronell [30]. Specifically, the AMX anion exchange membrane. Using the membrane properties provided by Kingsbury and Coronell and the permselectivity data reported in their work, good agreement was found between membrane model and experiments. The conditions for the simulations were the same as in [30], high concentration C_H of 0.5M in the high concentration compartment and a varying concentration in the low concentration compartment. No fit was necessary to have the membrane model closely predict the experimental results.